UNIVERSIDADE FEDERAL DO RIO GRANDE DO SUL
INSTITUTO DE INFORMÁTICA
PROGRAMA DE PÓS-GRADUAÇÃO EM COMPUTAÇÃO

VITOR FERNANDO PAMPLONA

Photorealistic Models for Pupil Light Reflex and Iridal Pattern Deformation

Thesis presented in partial fulfillment
of the requirements for the degree of
Master of Computer Science

Prof. Dr. Manuel M Oliveira
Advisor

Prof. Dr. Gladimir V. G Baranoski
Co-advisor

Porto Alegre, April 2008

CIP – CATALOGING-IN-PUBLICATION

Pamplona, Vitor Fernando

Photorealistic Models for Pupil Light Reflex and Iridal Pattern Deformation / Vitor Fernando Pamplona. – Porto Alegre: PPGC da UFRGS, 2008.

81 f.: il.

Thesis (Master) – Universidade Federal do Rio Grande do Sul. Programa de Pós-Graduação em Computação, Porto Alegre, BR–RS, 2008. Advisor: Manuel M Oliveira; Co-advisor: Gladimir V. G Baranoski.

1. Pupil-dynamics simulation. 2. Physiologically-based model. 3. Pupil light reflex. 4. Iridal pattern deformation. 5. Human visual system. 6. Face animation. I. Oliveira, Manuel M. II. Baranoski, Gladimir V. G. III. Title.

“Sete semanas? O Sr. é um fanfarrão, Sr. 01! O senhor tem sete dias, Sr. 01! ”

— CAPITÃO NASCIMENTO FACTS

ACKNOWLEDGMENTS

A special thanks goes to my advisors: Manuel Menezes de Oliveira Neto, who always help me to push my limits, teach me the "science-based way of life", who helped me in the experiments and for the great improvements in all six papers submitted during this program; and Gladimir V. G. Baranoski for pushing me toward the use of bio-physical references, for suggesting the idea of exploring the iris and for the great discussions along the period.

I am very grateful for resources, contributions and suggestions from Prof. Jacobo Melamed Cattan (Ophthalmology-UFRGS), who helped me dilating the pupils of several volunteers, and for letting me use the color videos from the Keratometer, Prof. Luis A. V. Carvalho (USP-SC) for videos of an infrared Keratometer and by exciting talks.

Thanks to Leandro A. F. Fernandes, Marcos Slomp, Eduardo Gastal and Denison L. M. Tavares who contributed in the demos and videos for papers generated by this work. Leandro Lichtenfelz (Mathematics-UFSC), Renato Silveira and Prof. Roberto da Silva, for the great help with advanced mathematical concepts and discussions. Ida Rossi (Librarian-UFRGS) for finding a lot of very old biological papers, Fernando Trebien and André Spritzer for english revisions and Cinara Cunha (Arts-FURB) for giving me permission to use her iris photo as a motivation of this work. I also thank the volunteers who allowed us to collect pictures and videos of their irises: Alex Gimenes, Boris P. Starov, Christian Pagot, Claudio L. Menezes, Giovane R. Kuhn, Leonardo Schmitz, Rodrigo Mendes, Tiago Etiene and specially João Paulo Gois who receive me at USP/São Carlos. Thanks to Microsoft Brazil for the financial support during the seven final months. Thanks to Prof. Paulo C. Rodacki (FURB) and Jomi Fred Hubner (FURB) for the recommendation letters and to Prof. Anatolio Laschuk to be ready when I needed help to record some videos at Hospital de Clínicas (University Hospital).

I would like to thank the professors Carla M.D.S. Freitas, João D. Comba, Luciana P. Nedel and Manuel M. Oliveira for their great work at UFRGS, for conducting the Computer Graphics Group to a level of excellence and to my colleagues of the Computer Graphics Group at UFRGS for providing an intellectually stimulating and enjoyable research environment. Fausto Blanco and Francisco de Moura Pinto for discussions about the academic and commercial ways of life and Fabio Bernardon for always saying that there is no practical utility in my work, holding my ego in a normal stage. To my family and all my friends, especially my parents Marli Knuth Pamplona and Carlos Fernando Pamplona (in memoriam), my brother Paulo Roberto Pamplona and my dogs Ayda, Magoo and Ully (in memoriam) for tolerating my absence of their lives.

I also thanks the people that take part of our soccer games and group parties, my neighbor Márcia M. Moraes and her family, and the cookies woman, Eliane, for giving me instants of a normal life even into a Master's program.

TABLE OF CONTENTS

LIST OF FIGURES

ABSTRACT

This thesis introduces a physiologically-based model for the pupil light reflex (PLR) and an image-based model for iridal pattern deformation. The PLR model expresses the pupil diameter as a function of the environment lighting, and is described by a delay-differential equation, naturally adapting the pupil diameter even to abrupt changes in light conditions. Since the parameters of the PLR model were derived from measured data, it correctly simulates the actual behavior of an average human pupil. The model is extended to include latency and constriction/dilation velocity, individual differences and some random noise to model hippus.

Another contribution of this work is a model for realist deformation of the iridal pattern as a function of pupil dilation and constriction. The changes in these patterns are tracked using photographs of irises from several volunteers taken during an induced pupil-dilation process. This data provided an estimate of the average behavior of the iridal features. The effectiveness and quality of the results are demonstrated by comparing the renderings produced by the models introduced in this thesis with photographs and videos captured from real irises.

The resulting models produce high-fidelity appearance effects and can be used to produce real-time predictive animations of the pupil and iris under variable lighting conditions. Combined, the proposed models can bring facial animation to new photorealistic standards.

Keywords: Pupil-dynamics simulation, Physiologically-based model, Pupil light reflex, Iridal pattern deformation, Human visual system, Face animation.

Modelos Fotorealistas para Dinâmica Pupilar em Função da Iluminação e Deformação dos Padrões da Íris

RESUMO

Este trabalho introduz um modelo fisiológico para o reflexo pupilar em função das condições de iluminação (*Pupil Light Reflex* - PLR), e um modelo baseado em imagem para deformação dos padrões da íris. O modelo para PLR expressa o diâmetro da pupila ao longo do tempo e em função da iluminação ambiental, sendo descrito por uma equação diferencial com atraso, adaptando naturalmente o tamanho da pupila a mudanças bruscas de iluminação. Como os parâmetros do nosso modelo são derivados a partir de modelos baseados em experimentos científicos, ele simula corretamente o comportamento da pupila humana para um indivíduo médio. O modelo é então estendido para dar suporte a diferenças individuais e a hippus, além de utilizar modelos para latência e velocidade de dilatação e contração.

Outra contribuição deste trabalho é um modelo para deformação realista dos padrões da íris em função da contração e dilatação da pupila. Após capturar várias imagens de íris de diversos voluntários durante diferentes estágios de dilatação, as trajetórias das estruturas das íris foram mapeadas e foi identificado um comportamento médio para as mesmas. Demonstramos a eficácia e qualidade dos resultados obtidos, comparando-os com fotografias e vídeos capturados de íris reais. Os modelos aqui apresentados produzem efeitos foto-realistas e podem ser utilizados para produzir animações preditivas da pupila e da íris em tempo real, na presença de variações na iluminação. Combinados, os dois modelos permitem elevar a qualidade de animações faciais, mais especificamente, animações da íris humana.

Palavras-chave: Simulação de dinâmica pupilar, modelo fisiológico, reflexo pupilar a luz, deformação de padrões da íris, sistema visual humano, animação facial.

1 INTRODUCTION

Arguably, the most important feature in facial animation are the eyes, which are essential not only in directing the gaze of the audience (LEE; BADLER; BADLER, 2002), but also in conveying the appropriate degree of expression through pupil dilation and constriction movements (WATT; WATT, 1992). Hence, for animations depicting close-up views of the face (Figure 1.1), natural-looking eyes and pupil movements are highly desirable.

> Walt Disney once said to his animation team that the audience watches the eyes and this is where the time and money must be spent if the character is to act convincingly (WATT; WATT, 1992).

Figure 1.1: Photograph of a human iris. Image courtesy of Cinara Cunha.

Differently from most of the body, the human eye is subject to some involuntary movements of the pupil, which are determined by ambient illumination, drug action, and emotional conditions, among others (REEVES, 1920; ELLIS, 1981; CALCAGNINI et al., 2000). Pupillary light reflex (PLR) is responsible for the constriction of the pupil area in highly lit environments and for its dilation in dimmed ones. Spontaneous irregular variations in pupil diameter are called hippus, occurring in a frequency range of 0.05 to 0.3Hz, oriented by the nervous system (TREVOR-ROPER; CURRAN, 1984; STARK, 1939). PLR and hippus are an integral part of our daily experience and, except for drug-induced action, is probably the single most noticeable of such involuntary movements of the pupil. Many other factors affect pupil size, including respiratory and heart rate (CALCAGNINI et al., 2000) particular states of mind, such as interest and curiosity (HESS; POLT, 1964), spectral sensitivity (WERNER, 2003) and spatial patterns in the visual field (LI; LIANG;

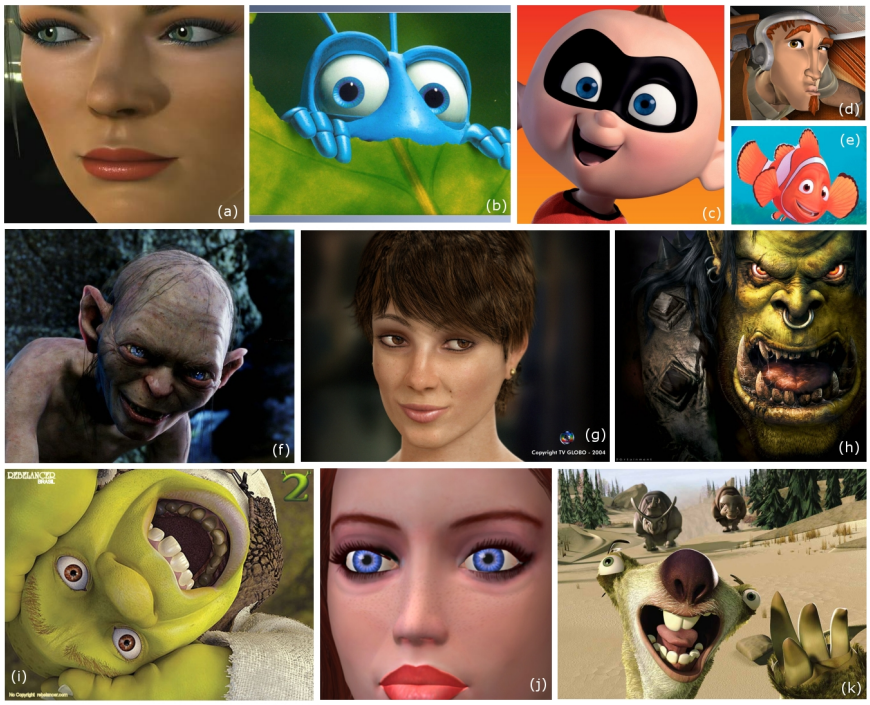

Figure 1.2: Examples of close up scene in recent movies/animations: (a) Nvidia's model, Adrianne (nVidia nZone, 2007); (b) Flik in Bug's Life (SfondiDelDesktop.com, 2007); (c) Jack-Jack in The Incredibles (PIXAR, 2007a); (d) Monkey from Acceleracers (HOT WHEELS, 2007); (e) Marlin from Finding Nemo (PIXAR, 2007b); (f) Gollum from Lord of the rings (MMVII New Line Productions, 2004); (g) Eva Byte, presenter of Fantástico at TV Globo (GLOBO, 2004); (h) Orc from Warcraft game (ESCALOFRIO.FREE.FR, 2007); (i) Shrek in Shrek 2 (REBELANCER, 2007); (j) Face from a simple blender tutorial (JCH DIGITAL DESIGNS, 2007); (k) Sid from Ice Age (TWENTIETH CENTURY FOX, 2006).

SUN, 2006). Taking all these aspects into account seems to be impractical due to their inherent complexity and limited supporting data.

The human iris is a muscular tissue containing several easily identifiable structures, such as the collarette, pigment spots, and crypts (Figure 1.1). Together, they define patterns, believed to be unique to each person (DAUGMAN, 2002), that are deformed as a result of changes in the pupil diameter. Although pupil light reflex and iridal deformations could be animated using standard computer graphics techniques, such as parametric representations controlled by velocity curves, the use of physiologically-based models guided by physically meaningful parameters can make the process more predictable and automatic, which, in turn, may result in more realistic and reproducible animations of these movements.

This thesis presents a physiologically-based model for realistic animation of pupil dynamics and iridal pattern deformation. The model combines some theoretical results from the field of Mathematical Biology (LONGTIN; MILTON, 1989) with experimental data collected by several researchers relating pupil diameter to the intensity of environmental light (MOON; SPENCER, 1944). The proposed model is extended to support individual differences, hippus simulation and latency and velocity models. The resulting model produces high-fidelity appearance effects and can be used to produce real-time predictive animations of the pupil and iris under variable lighting conditions (Section 5.5). The

process iridal pattern deformation was modeled by acquiring a set of high-resolution photographs of real irises at different levels of pupillary dilation and by tracking their features across the set of images. By analyzing the tracked positions, a simple analytical expression for the iridal pattern deformation as a function of the pupil diameter was obtained (Section 6). To the best of our knowledge, these models are the first physiologically-based model for simulating pupil light reflex presented in the graphics literature (the first model ever to simulate individual variability in terms of PLR sensitivity - Section 5.4), as well as the first model for iridal pattern deformation. The effectiveness and quality of the models are demonstrated by comparing the results with photographs and videos taken from real irises(Figure 1.3).

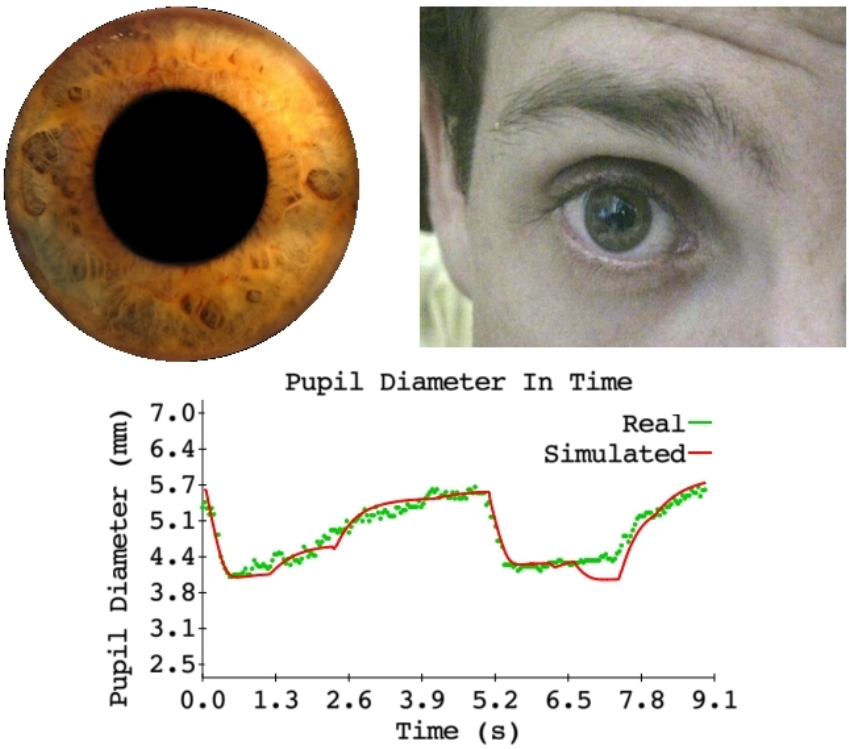

Figure 1.3: The comparison of the proposed models with real irises: (Top-Left) the results of the proposed pupil light reflex and iridal pattern deformation models; (Top-Right) A frame from a nine-second-long video sequence showing a human iris exposed changes in lighting conditions; (Bottom) a graph comparing the pupil diameter as a function of time. The dots represent the values manually measured for each frame of the video sequence. The solid line shows the simulated results obtained with our PLR model. Note how the simulated results satisfactorily predict the real ones.

1.1 Structure of this Thesis

The remaining of this thesis is organized as follows: Chapter 2 discusses some techniques for image synthesis of the human iris and eye. Chapter 3 reviews the anatomy and physiology of the eye and presents a mathematical model for iris structure. Chapter 4 presents models for pupillary movements, latency and constriction/dilation velocity. Chapter 5 introduces the model for pupil light reflex, and extensions to model hippus and individual differences. Chapter 6 presents the image-based model for iridal pattern defor-

mation. Chapter 7 discusses an application example showing a human face rendered using the proposed models to simulate the pupil and iridal responses to the environmental light. Finally, Chapter 8 summarizes the thesis and lists some avenues for future exploration.

2 RELATED WORK IN COMPUTER GRAPHICS

A few researchers have addressed the issue of realistic human iris synthesis. Lefohn *et al.* (2003), based on ocularist knowledge, created a model for the human iris blending[1] several layers of semi-transparent textures, each one containing some eye feature, mapped in cones. (Figure 2.1). The textures are created by artists and carry no information about the physiology of the iris.

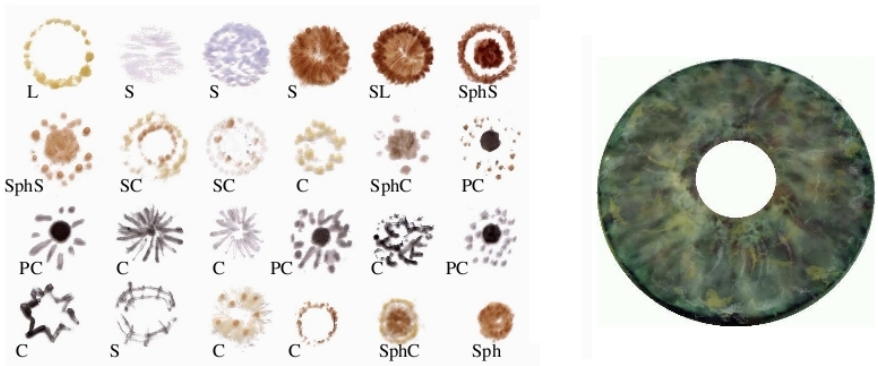

Figure 2.1: Results from Lephon *et al.*: (left) Example textures containing Stroma (S), collarette (C), limbus (L), pupil (P) and sphincter muscle (Sph) components; (right) The final synthetic iris. From (LEFOHN et al., 2003)

Other image-based approaches have been proposed by Cui *et al.* (2004), Wecker *et al.* (2005) and Makthal and Ross (2005). Essentially, they decompose a set of iris images using techniques such as principal component analysis[2] (CUI et al., 2004), multi-resolution and wavelets[3] (WECKER; SAMAVATI; GAVRILOVA, 2005) and Markov random fields[4] (MAKTHAL; ROSS, 2005), and recombine the decomposed data to generate new images of irises. The algorithm proposed by Wecker *et al.*. needs a pre-processing stage where the center of the pupil and the iris are aligned and the pupil is removed. Also, the algorithm can only join images with equal features, as the number of high-frequency rings that were created by folds, for example. The algorithm from Makthal and Ross mix user-defined iris features cutted from iris images. It needs an user interaction to stop the iterator when a good iris image is rendered (Figure 2.2).

[1] A weighted sum, pixel-by-pixel, over two or more semi-transparent images.

[2] A transformation where the data set receives a new coordinate system, in which new axes follow the direction of greatest variance in the data set. (CUI et al., 2004)

[3] Orthonormal basis functions. (WECKER; SAMAVATI; GAVRILOVA, 2005)

[4] Models used to describe the probability distribution governing the intensity values of pixels in a specific

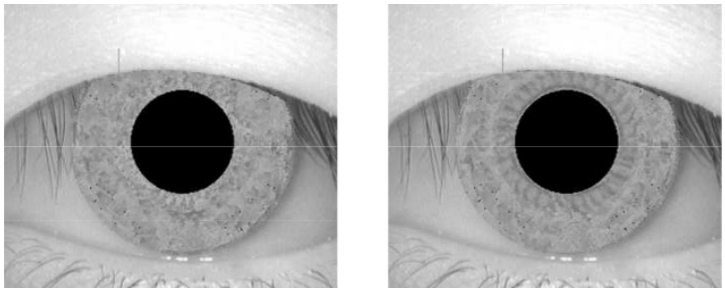

Figure 2.2: Two iris synthesized by Makthal and Ross method. From (MAKTHAL; ROSS, 2005)

Zuo and Schmid (2006; 2006) created a 3D model of the iris fibers. Each fiber is a continuous 3D curve in cylindrical coordinates, which is rendered using the conventional graphics pipeline (Figure 2.3). A final Gaussian-blur step is applied to the resulting image, which is then used to represent the iris.

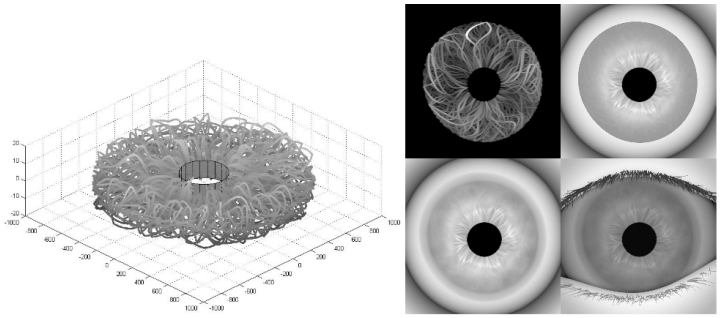

Figure 2.3: Results from Zuo and Schmid: (left) the 3D model for the collagen fibers; (right) The four steps of the algorithm: (i) projection of the fiber in image space; (ii) adding a semitransparent top layer with an irregular edge to simulate the collarette; (iii) blurring the root of the iris and add a noise layer; (iv) adding eyelids and eyelashes to the final synthetic iris. From (ZUO; SCHMID, 2006)

Lam and Baranoski (2006) introduced a predictive light transport model for the human iris, which computes the spectral responses of iridal tissues described by biophysical parameters. As the result, their model predicts the color of the iris using subsurface scattering techniques [5]. Although they use a simplified structure of the iris to test the model, a detailed structure can generate highly detailed images of the iris.

Finally, François *et al.*. (2008; 2007) proposes a model to recover an approximate representation for the relief of a given iris and use subsurface scattering to render it. They make the assumption that the light scatters more in thicker regions of the iris and scatters less in thinner regions. Given a picture of an iris, they assume that, darker parts represent thinner parts of the iris and lighter parts, the ticker ones. They use gray scale values of an iris picture to generate a height map[6], whose rendering allows, in close up

neighborhood (MAKTHAL; ROSS, 2005).

[5]A set of simulation techniques which the light penetrates the surface of a translucent object and is scattered by interacting with the material.

[6]An image where each pixel stores a height value. When associated to an object, the rendering process will add the height value to the 3D position in the object surface associated to that pixel.

views, the perception of shadows (Figure 2.4). As a future work, François *et al.*. intent to recover, from iris images, the respective densities of eumelanin and pheomelanin pigment found in Stromal and ABL layers (discussed in Chapter 3), needed by Lam and Baranoski model (2006).

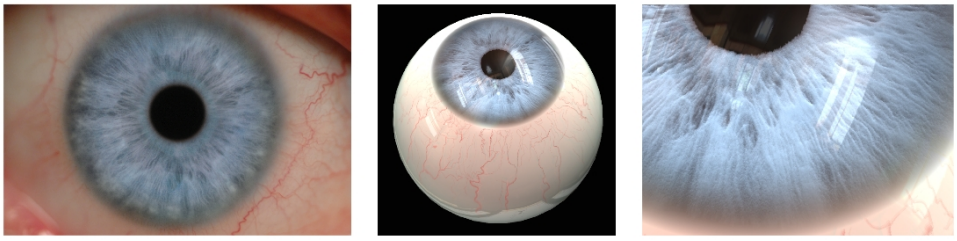

Figure 2.4: Results from François *et al.*: (left) Eye picture captured with polarizing filters to avoid corneal reflections; (middle) Rendering of the resulting iris model using the estimated height field; (right) Close up showing shadows. Images from (FRANÇOIS et al., 2008).

Sagar et al. (1994) developed an anatomically detailed model of the eye to be used in a surgical simulator. In their model, Gaussian perturbations were used to simulate the waviness of ciliary fibers and the retraction of pupillary fibers during pupil dilation. Alternatively, depending of the level of object manipulation, a texture mapping[7] approach was used to model the iridal appearance. It is worth noting, however, that their goal was to achieve functional realism (FERWERDA, 2003) as opposed to physical or photorealism.

All these models and techniques, however, do not handle pupillary movements nor deformation of iridal patterns.

[7] A technique of mapping pixels of an image to 3D positions in the surface of an object.

3 AN OVERVIEW OF THE HUMAN IRIS AND PUPIL

This chapter presents an overview of the human eye, describing the anatomy and physiology of the iris. Its goal is to familiarize the reader with terminology and some biological properties that will be relevant in the following chapters.

The eyes are a fundamental part of the visual system found in many organisms. They can vary from the simplest eye which only detects light or dark to the complex ones with 350 degrees of field of view. The eye translates electromagnetic radiation (light), from different wavelengths and intensities, to neural action potentials and sends them to the brain. Figure 3.1 shows the anatomy of the human eye.

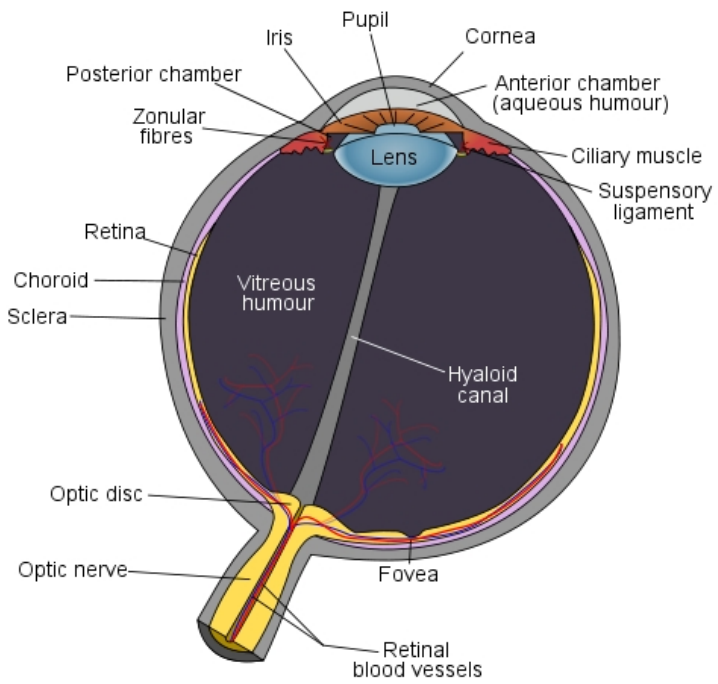

Figure 3.1: A sketch of the human eye internal structures. Source (WIKIPEDIA: the free encyclopedia, 2007).

In humans, the electromagnetic radiation enters in the eye by the cornea, an elliptic transparent layer with a refractive power of 43 diopters, roughly two-thirds of the eye's total refractive power (PROENÇA, 2006; BORES, 2002; BERG; TAN, 1994). The cornea is connected to the sclera, the white part of the eye. It contains collagen fibrils and elastin,

just like the sclera, but has also a protein called keratin, that makes it transparent. Cornea and sclera protects other internal structures of the eye (BORES, 2002).

Behind the cornea, there is a thick watery substance called aqueous humour, constantly produced by the ciliary process inside the ciliary body and drained by the trabecular meshwork. It is responsible for providing nutrients to the lens and cornea (BORES, 2002). The Lens (also called crystalline lens) is a transparent, biconvex and flexible (lentil-shaped) structure with 15 diopters. It has from 7 to 9 mm of diameter and from 2 to 4.5 mm of depth (SCHACHAR, 2005). Its curvature and thickness are changed by the ciliary muscle to adjust the focal distance during the accommodation. The aqueous humour let pass wavelengths from 220 nm and 2400nm, however after 980nm they are gradually absorbed. This process is independent of age (BOETTNER; WOLTER, 1962). In the other side, the lens are affected by the age and the ratio of direct light transmission decreases along time (i.e. while a baby perceives wavelengths starting at 300 nm, an adult can only perceive wavelengths starting at 400nm on average) (BOETTNER; WOLTER, 1962; SCHMID et al., 2004).

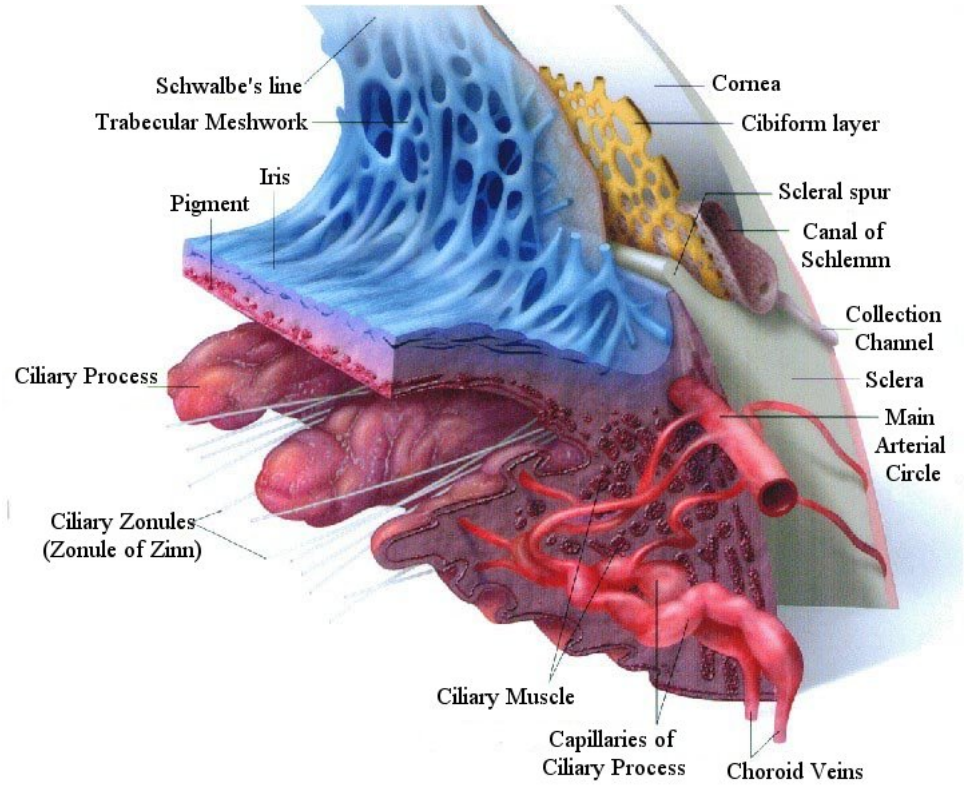

Figure 3.2: A sketch of the connection between the iris and the sclera inside the human eye. Source (DECKERT, 2007).

The retina, located in the posterior part of the eye, is the sensory element of the pupillary system, consisting approximately of 130 millions of photo-receptors (rods and cones). It converts electromagnetic radiation, already disturbed by other tissues of the eye, to neural potentials. After the ganglion retinal cells, the pulses pass through sustained X cells, which act as a low-pass filters, and transient Y cells, which are high-pass filters (PRIVITERA; STARK, 2006), and then, they are sent to the brain through the optic nerve (TREVOR-ROPER; CURRAN, 1984). The illuminance reaching the retina is measured in Troland (Td) which means the photo luminance cd/m^2 multiplied by pupil area (m^2).

3.1 The Iris

The human iris has a diameter of about 12mm forming a disc. It controls how much light reaches the retina and divides the two aqueous filled compartments, of the anterior and posterior eye chambers. Under high levels of lighting, the iris dilates, flattening itself and decreasing the pupil size. Under low levels of illumination, it constricts, folding itself and increasing the pupil area. The pupil diameter varies from 1.5mm to 8mm on average (REEVES, 1920), and, in general, it is not a perfect circle. Also, its center may deviate from the center of the iris by an offset of up to 20%, generally to nasal side (FREDDO, 1996).

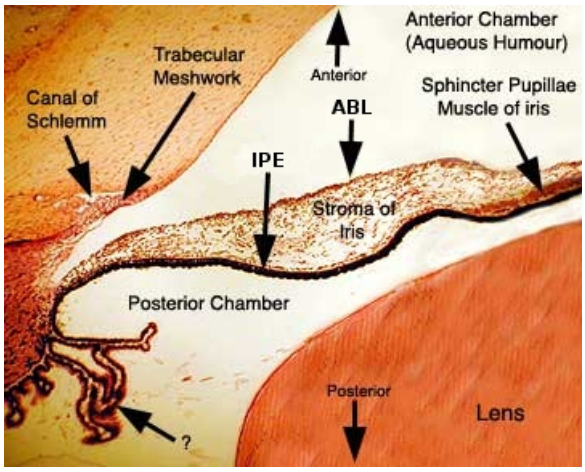

Figure 3.3: A sketch showing the dilator muscle, the sphincter muscle, ABL, Stromal Layer and IPE. Extracted from (BELL, 1999)

As showed in Figure 3.3, the iris is a vascularized structure and consists of three layers: (i) *anterior border layer* (ABL) composed by a dense arrangement of pigmented cells (melanocytes), collagen fibers and fibroblasts; (ii) *stromal layer*, a neuro-vascular tissue very similar to ABL but loosely arranged; and (iii) *iris pigmented epitelium* (IPE), a highly pigmented tissue made with epithelial cells forms an opaque layer (IMESCH; WALLOW; ALBERT, 1997). The color of the iris is determined by the pigmentation density, the quantity of hemoglobins and carotenoids, and the scattering processes in the ABL and stromal layers (i.e. blue irises are a result of absorption of long wavelength light and reflection of shorter wavelengths by the iris tissues) (BARANOSKI; LAM, 2007; FREDDO, 1996). Ambient illumination can change the iridal color as showed in Figure 3.4.

The human iris is also divided in two zones by the *collarette*, a delicate zig-zag line also known as the iris frill (Figure 3.5). The *pupillary* zone is the boundary area next to the pupil. The *ciliary* zone extends from the outer border of the iris to the collarette. Each zone is characterized by a muscle in the stromal layer. The *sphincter*, located in the pupillary zone inside the IPE layer and closest to Stroma, is a circumferentially oriented thin smooth muscle that constricts to decrease the pupil size. The *dilator*, found in the ciliary zone, is a radial muscle that constricts to increase the pupil size. Figure 3.5 shows three visible features of the iris, formed by the collagen fibers which has no genetic penetrance: (1) thin regions called crypts (also called Crypts of Fuchs), (2) the collarette and (3) highly dense pigment spots or moles, appearing randomly over the ciliary zone. There are three other visible features: (i) concentric furrows in ciliary zone, folds made by the

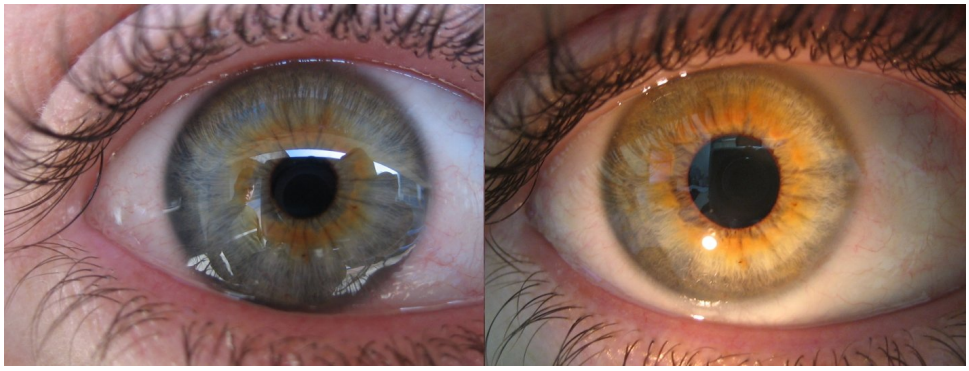

Figure 3.4: Two photographs of the same eye under different illumination conditions. The image on the left was taken under natural lighting while the image on right was illuminated with a flashlight

dilator muscle during the contraction; (ii) radial furrows closest to the pupil and (iii) the pupillary ruff located at the pupillary margin, formed by a visible part of IPE.

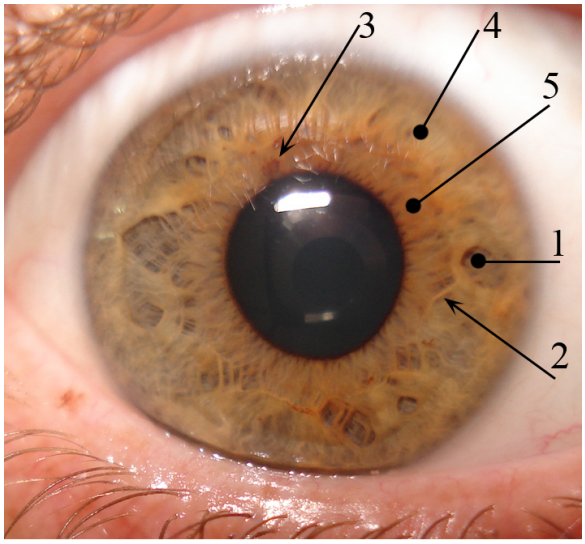

Figure 3.5: Photograph of a human iris. The numbers indicate: (1) crypt, (2) collarette, (3) pigment spot, (4) ciliary zone and (5) pupillary zone

The sphincter and dilator muscles are independently connected to the autonomous nervous system (ANS) (TILMANT et al., 2003; KRENZ et al., 1985). The sphincter is innervated by parasympathetic nerves (PNS) while the dilator is innervated by sympathetic nerves (SNS). In such an arrangement, the two muscles move autonomously. The parasympathetic and sympathetic pathways are distinct and never cross, so the pupil size results from a balance of the separately incoming stimuli to the two muscles (BERGAMIN et al., 1998). The Parasympathetic neural pathway, for example, starts on the retina, pass through the Edinger-Westphal nuclei and ends on the iris muscle (Figure 3.6) (PRIVITERA; STARK, 2006).

The pupil moves in according to two actions: pupil light reflex (PLR), the pupil response for light reaching the retina and accommodation, the pupil response for focal length. There is also some involuntary variation called *hippus*. The ANS conducts the PLR and hippus actions. Accommodation pulses, however, do not affect the iridal mus-

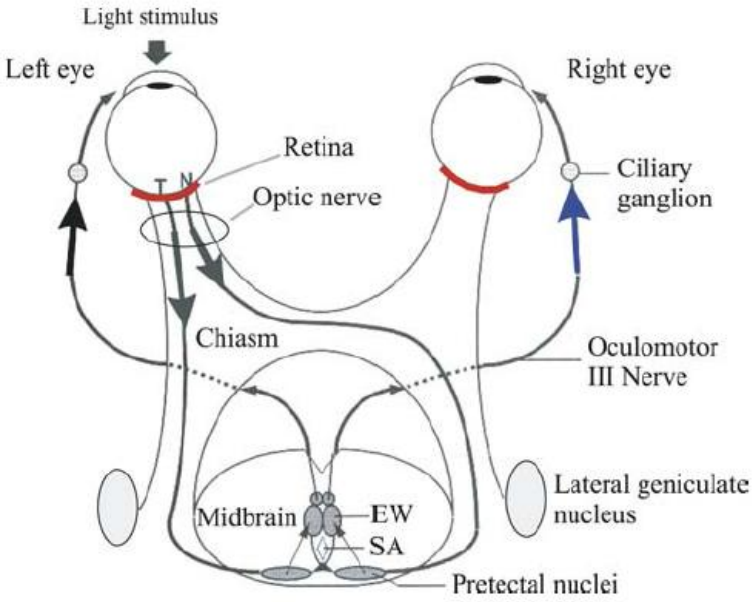

Figure 3.6: Parasympathetic neural pathway of pupil light reflex. The Parasympathetic neural pathway starts on the retina, pass through the Edinger-Westphal nuclei and ends on the iris muscle. Source: (PRIVITERA; STARK, 2006)

cles directly, only the ciliary muscle, which is located in the root of the iris suspending the lens (TAMM; TAMM; ROHEN, 1992). During PLR, when light reaches the retina, neural signals are sent by the SNS and the PNS pathways to the brain, which sends back a signal for closing or opening the pupil. PLR can be modeled in two phases: perception and, after some time delay, an adjustment. It is also an example of a negative feedback system (PINGNET et al., 1988), since an increase of light will cause a decrease of pupil size.

Several researches found external factors that affect pupil size though PLR, accommodation or hippus: lighting (REEVES, 1920; ELLIS, 1981; STILES; CRAWFORD, 1933; MOON; SPENCER, 1944; POKORNY; SMITH, 1995), focal length (KASTHURIRANGAN; GLASSER, 2005; SCHOR; BHARADWAJ, 2005), spatial patterns in visual field (UKAI, 1985; LI; LIANG; SUN, 2006; LI; SUN, 2005; REEVES, 1920), respiratory and heart rate (YOSHIDA et al., 1994, 1995; CALCAGNINI et al., 2000), particular states of mind and emotional factors, such as interest and curiosity (HESS; POLT, 1964; PEASE; PEASE, 2004), drugs and diseases (BERGAMIN; ZIMMERMAN; KARDON, 2003; KOJIMA et al., 2004), age (STRAUB; THIES; KERP, 1992; WINN et al., 1994), iridal color (BERGAMIN et al., 1998), spectral sensitivity (WERNER, 2003), and even the exact region on the crystalline lens reached by an incident light beam, called Stiles-Crawford effect (STILES; CRAWFORD, 1933). Taking all these aspects into account, when designing a physiologically-based model for the pupil size, seems to be impractical due to their inherent complexity and limited supporting data.

3.2 Biological Iris Structure Models

Although the iris is a well-known structure in the biological field (FREDDO, 1996), the literature seems to contain no analytical model describing its behavior. According to

Wyatt (2000), Rohen (1951) seems to have been the been the first researcher to study the form of the collagen structure of the iris. He proposed a model for the collagen fibers in which they are arranged in a series of parallel arcs, connecting the iris root with the pupil border, clockwise and counterclockwise in an angle of 90 degrees oriented by the center of the pupil (Figure 3.7). These fibbers are interwoven with other iris components like blood vessels.

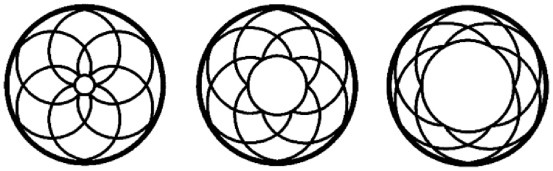

Figure 3.7: The collagen arrangement in a series of parallel arcs model proposed by Rohen (1951). Image source: (WYATT, 2000)

Newsome and Loewenfeld (1971) studied iris details such as the thickness and course of iris vessels, the size and shape of crypts and the position of the folds step by step, from larger to smaller pupils. According to them, there are no observable differences in the iris regarding light-induced or drug-induced pupil dilation/constriction. The ciliary zone grew steadily each step, but in contrast the surface area of the pupillary zone did not change until the pupil is quite small. This means that the ciliary zone is deforms linearly, while the pupillary zone in a non-linear way. They also found lower and higher limits for this non-linearity. However, the article points to possible errors in accuracy, specially when the pupil size is large.

Based on the fibber arrangement proposed by Rohen, Wyatt (2000) derived equations that minimize the wear and tear of the collagen fibbers and created a non-linear 2D mathematical model for iris deformation. However, Wyatt did not consider iridal folds and validated his model with canine, porcine and monkey iris. Although this model was already used by iris recognition systems (WEI; TAN; SUN, 2007; YUAN; SHI, 2005), there are no studies indicating that Wyatt's model can be applied to human iris (WYATT, 2007). Nevertheless, Wei *et al.* (2007) and Yuan (2005) applied the Wyatt's model to human iris recognition systems, reducing the recognition error by 0.2% and 0.3% respectively.

3.3 Summary

This chapter presented a brief overview of the iris structure, and its neural system and actions. Such a description was intended to provide just enough information to familiarize the reader with some concepts and terminology that will be used in the next chapters, such as the notions of pupil light reflex and its associated delay. An in-depth description of these subjects is beyond the scope of this thesis and can be found in many good medical literature sources (TREVOR-ROPER; CURRAN, 1984).

4 MODELS OF PUPIL DYNAMICS

This chapter provides an overview of key models designed to assist the analysis of PLR and hippus movements. These models take into account, either explicitly or implicitly, a number of physical parameters related to these phenomena: (i) *latency*, (ii) the *constriction velocity*; (iii) the *dilation velocity*; (iv) the *maximum pupil size*; and (v) the *minimum pupil size*. The models described here form the basis of the proposed physiologically-based PLR model that will be presented in chapter 5.

4.1 Empirically-Based Models

The pupillometry literature describes several models built around experiments designed to measure the values of some parameters as a function of incident light intensity. Link and Stark (1988) performed a study where a light source was placed in front of the subject iris and, by varying the intensity and frequency of the light, they measured the pupillary latency, a time delay between the instant in which the light pulse reaches the retina and the beginning of iridal reaction due nerve transmission, neuro-muscular excitation and activation delays. Their results are summarized in the model represented by Equation 4.1, no information about how many subjects took part in the experiment has been provided.

$$\tau(R, L_{fl}) = 253 - 14\,ln(L_{fl}) + 70R - 29\,R\,ln(L_{fl}) \tag{4.1}$$

where τ is the latency, L_{fl} is the luminance measured in foot-Lamberts (fL), and R is the light frequency measured in Hz.

Ellis (1981) performed a similar experiment (without considering the light frequency) with 19 volunteers to find three equations that provide the average latency, and maximum constriction and dilation velocities for a given light source intensity. These equations are given by

$$\tau(L_{cd}) = 445.7 - 22.9L_{cd} + 76.2L_{cd}^2 \tag{4.2}$$

$$V_c(L_{cd}) = 0.15 + 2.0L_{cd} - 0.17L_{cd}^2 \tag{4.3}$$

$$V_d(L_{cd}) = 0.16 + 0.72L_{cd} - 0.07L_{cd}^2 \tag{4.4}$$

where τ is expressed in ms, V_c and V_d are expressed in mm/s, and L_{cd} is the intensity of the light, measured in $candelas/m^2$. Figure 4.1 shows a comparison between the latency models from Ellis (Equation 4.2) and Link and Stark when $R = 0.4$ (Equation 4.1).

Similar models (MOON; SPENCER, 1944; GROOT; GEBHARD, 1952; POKORNY; SMITH, 1995) predict an average pupil size as a function of the light intensity based

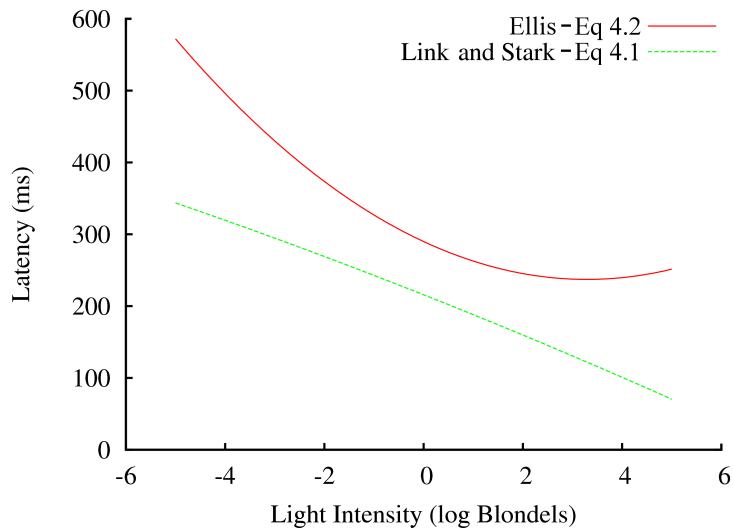

Figure 4.1: Comparison between latency models from Ellis (Equation 4.2) and Link and Stark when $R = 0.4$ (Equation 4.1).

on a few experimental measurements and using the previous available data. In those experiments, each subject is seated in front of a white screen which fills most of his/her field of view. A uniform light intensity on the screen affects the pupil diameter, which is measured after it reaches an equilibrium state. For instance, Moon and Spencer (1944) examined the available data (17 subjects) and proposed a model for the pupil size of an individual average, that is given by

$$D = 4.9 - 3tanh\left[0.4(log_{10}(L_b) - 0.5)\right] \tag{4.5}$$

where the pupil diameter D varies from 2 to 8 mm, and the background luminance level L_b varies from 10^5 blondels in sunny days to 10^{-5} blondels in dark nights. Today, the model proposed by Moon and Spencer is the most cited pupil-size model in the literature.

The de Groot and Gebhard model (1952) was based in experiments involving 43 subjects and is expressed as:

$$D = 10^{(0.8558 - 0.000401(log_{10}(L_a) + 8.1)^3)} \tag{4.6}$$

where the background luminance level L_a is measured in millilamberts (mL). The Pokorny and Smith model is expressed by Equation 4.7:

$$D = 5 - 3 * tanh(0.4 * (log_{10}(L_{cd}))) \tag{4.7}$$

Here, the luminance L_{cd} is measured in candelas per square meter (cd/m^2). Figure 4.2 compares the three models.

4.2 Physiologically-Based Models

In Mathematical Biology and related fields, models based on physiological and anatomical observations were derived to express the relationships among the pupillary action variables without relying on quantitative experimental data. For example, Usui and Stark (1982) proposed a parametric model of the iris to describe the static characteristics of pupil response to light stimuli, and to explain its random fluctuations in terms of probability

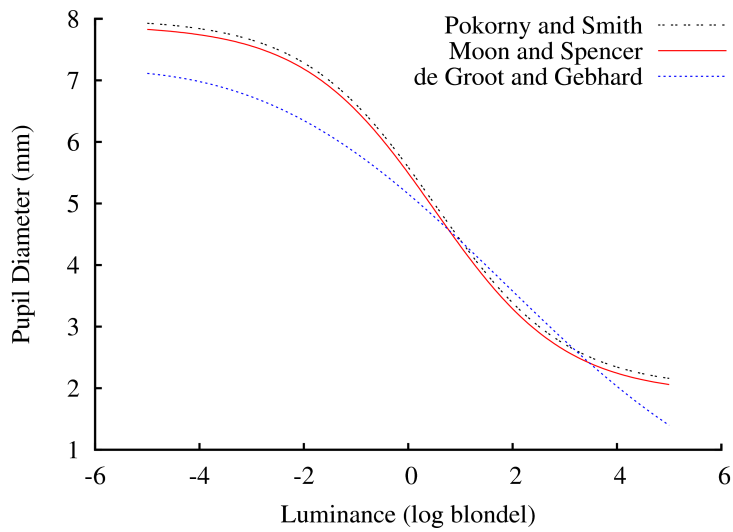

Figure 4.2: Pupil diameter models as a function of luminance expressed in cd/m^2. The compared models are: de Groot and Gebhard (1952), Moon and Spencer (1944), and Pokorny and Smith (1995).

density functions. Recently, Tilmant *et al.* (2003) proposed a PLR model based on physiological knowledge and guided by experiments. Although they have obtained plausible results, Tilmant *et al.* have recommended the use of another physiologically-based model to monitor more accurately pupillary dynamics, namely the time-dependent model developed by Longtin and Milton (1989), which, models the dynamic non-linear behavior of the pupil using a delay-differential equation. Delay-differential equations (DDEs) are a special kind of differential equations whose solutions involve past values of the state variable (NORBURY; WILSON, 2000).

The Longtin and Milton's equation describes the neural ANS pathways, presented in the section 3.1, to pupillary light reflex. Assuming that all the light reaching the retina is converted to action potentials, Longtin and Milton describe the efferent neural signal $E(t)$ arriving at the iris per unit of time t, as

$$E(t) = \beta \, ln \left[\frac{\phi(t-\tau)}{\bar{\phi}} \right] \tag{4.8}$$

where β is a constant of proportionality and ϕ is the retinal light level measured in lumens and defined by Stark and Sherman (1959) as $\phi = IA$: illuminance (I in lumens/mm^2) times the pupil area (A in mm^2), τ is the latency, and $\bar{\phi}$ is the retinal light level threshold (*i.e.*, the light level below which there is no change in the pupil area). The notation $\phi(t-\tau)$ indicates that the current effect depends on the retinal light flux at a time τ units in the past (latency). The delay is calculated with the same physiological parameters using equations presented in the Section 4.1. As the efferent neural signal reaches the iris, it induces some muscular activity x that may cause the pupil to dilate or constrict. According to Partridge and Benton (1981), the relationship between $E(t)$ and x can be approximated by

$$E(t) \tilde{=} k \left(\frac{dx}{dt} + \alpha x \right) \tag{4.9}$$

where k is a proportionality factor and α is a rate constant that depends on the definition and units of x used in the model. Longtin and Milton (1989) combine Equations 4.8

and 4.9 as

$$\frac{dx}{dt} + \alpha x = \gamma \, ln \left[\frac{\phi(t-\tau)}{\bar{\phi}} \right] \tag{4.10}$$

They express the pupil area A as $A = f(x)$ and use the inverse $f^{-1}(A) = g(A) = x$ to remove x from Equation 4.10. In their paper, Longtin and Milton use a Hill function (HILL, 1938) (Equation 4.11) as the function f, since it can approximate the elasto-mechanical properties of the iris during the pupillary activity:

$$A = f(x) = \frac{\Lambda \theta^n}{\theta^n + x^n} + \Lambda' \tag{4.11}$$

here, Λ' and $\Lambda + \Lambda'$ are, respectively, the minimum and the maximum pupil areas, and θ is the value of x corresponding to the average pupil area. The Longtin and Milton's model then becomes (LONGTIN; MILTON, 1989):

$$\frac{dg}{dA}\frac{dA}{dt} + \alpha g(A) = \gamma \, ln \left[\frac{\phi(t-\tau)}{\bar{\phi}} \right] \tag{4.12}$$

where

$$g(A) = x = \sqrt[n]{\frac{\Lambda \theta^n}{A - \Lambda'} - \theta^n} \tag{4.13}$$

It is worth noting that similar functions ("S-shaped" curves) relating pupil size to different illumination levels have been proposed by physiologically-based models (*e.g.*, the model devised by Usui and Stark (1982)) and empirically-based models (*e.g.*, the model devised by Moon and Spencer (1944)) to approximate static pupil responses, *i.e.*, under constant illumination conditions.

4.3 Summary

This Chapter presented the most important empirical and physiologically-based models for pupil dynamics. Among those, the models of Moon and Spencer, and Longtin and Milton are the most regarded ones in the literature. They form the basis of the proposed physiologically based model that will be described in Chapter 5.

5 THE PROPOSED PHYSIOLOGICAL-BASED MODEL

This Chapter presents the main contribution of this thesis: the physiological-based time-dependent model for pupil light reflex, which supports individual differences, and is represented by a delay-differential equation (DDE). The Chapter also compares the results obtained with the proposed model against some videos and photographs captured from real human irises.

The model of Moon and Spencer (Equation 4.5) is based on a set of discrete measurements and represents the response on an average individual under various lighting conditions. The measurements have been made after the pupil size has stabilized for the given set of illumination levels and, therefore, their model does not describe the pupil behavior outside the equilibrium state. Moreover, pupil size, latency, constriction and re-dilation velocities tend to vary between individuals exposed to the same lighting stimulus (MOON; SPENCER, 1944; WINN et al., 1994), something that is not captured by the model of Moon and Spencer.

Longtin and Milton's model (Equation 4.12) is time-dependent and adaptive, with the potential to handle abrupt lighting changes. It is a theoretical model and, unfortunately, Longtin and Milton did not provide the values for the various parameters in their model (*i.e.*, γ, α, θ, n, $\bar{\phi}$), as these, in principle, depend on the abstract notion of iridal muscular activity, individual differences, as well as on the use of the Hill function. The use of incorrect parameter values will not produce realistic results and may cause Equation 4.12 not to converge.

Starting from the Longtin and Milton's and from Moon and Spencer's models, a practical model that predicts the pupil diameter for the non-equilibrium case based on experimental data is derived (Section 5.2). Section 5.4 shows how the basic model can be extended to take individual variability into account.

The goal is to be able to exploit the flexibility of the Longtin and Milton model while replacing the Hill function with the human-pupil-specific experimental data that forms the basis of the Moon and Spencer model. In order to show how this can be done, a series of algebraic manipulations on the expressions of both models will be made until recover the desired parameter values simply by comparing the two resulting expressions.

5.1 Equilibrium Case

Under constant lighting conditions, the pupil area in the Longtin and Milton's model will converge to an equilibrium state, where

$$\frac{dg}{dA}\frac{dA}{dt} = 0$$

Under such circumstance and assuming there is no occurrence of hippus, ϕ becomes time-invariant. Also, recall that $ln(m/n) = ln(m) - ln(n)$ and, therefore, one can rewrite the Longtin and Milton model (Equation 4.12) for the equilibrium case as:

$$\alpha g(A) = \gamma \left(ln(\phi) - ln(\bar{\phi})\right) \tag{5.1}$$

In turn, the Moon and Spencer model can be written as

$$\left(\frac{D-4.9}{3}\right) = -tanh\left[0.4\left(\frac{ln(L_b)}{ln(10)} - 0.5\left(\frac{ln(10)}{ln(10)}\right)\right)\right]$$

and since the hyperbolic tangent is an odd function, one can rewrite the above equation as

$$-2.3\ atanh\left(\frac{D-4.9}{3}\right) = 0.4(ln(L_b) - 1.1513) \tag{5.2}$$

where $atanh$ is the arc-hyperbolic tangent. Comparing Equations 5.1 and 5.2, in order for the Longtin and Milton's model to fit the response of Moon and Spencer's average subject under the equilibrium conditions, one has

$$-2.3\ atanh\left(\frac{D-4.9}{3}\right) \approx \alpha g(A) \tag{5.3}$$

$$0.4(ln(L_b) - 1.1513) \approx \gamma(ln(\phi) - ln(\bar{\phi})) \tag{5.4}$$

From Equation 5.4 one can estimate the value of the parameter γ. One should note, however, that L_b is expressed in blondels (luminance) while ϕ is given in lumens (illuminance). For a perfect (lambertian) diffuse reflector, 1 blondel = 10^{-6} lumens/mm^2 (OHTA; ROBERTSON, 2005). Since the light flux ϕ depends on the area of the pupil, in order to estimate γ, one first evaluate the left-hand side of Equation 5.4 for the entire range of illumination covered by the Moon and Spencer's model: $L_b \in [10^{-5}, 10^5]$ blondels. For each value of L_b, one then use Equation 4.5 to estimate D, from which the pupil area $A = \pi(D/2)^2$, and then ϕ, are computed. The retinal light level threshold $\bar{\phi}$ = 4.8118×10^{-10} lumens was obtained using the pupil diameter $D_t = 7.8272$ mm, predicted by Equation 4.5 for $L_b = 10^{-5}$ blondels. Using the tabulated data for the left-hand side of Equation 5.4 and the conversion scheme just described, one get the following fitting:

$$0.4(ln(L_b) - 1.1513) \approx 0.45\ (ln(\phi) - ln(\bar{\phi})) - 5.2 \tag{5.5}$$

whose quality of the approximation is illustrated in Figure 5.1 (left). The vertical axis of the graph (scaled muscular activity) represents $\alpha g(A)$, where $g(A) = x$ is the muscular activity. The extra constant -5.2 translates the function on right-hand side of Equation 5.4 vertically, improving the fitting. Given Equation 5.5, one can replace $g(A)$ with $M(D)$ (Equation 5.3), with $\alpha = -2.3$, where $M(D)$ is given by

$$M(D) = atanh\left(\frac{D-4.9}{3}\right) \tag{5.6}$$

Thus, the equilibrium situation can be expressed by Equation 5.7. As expected, it approximates the Moon and Spencer's function (Equation 4.5) for the pupil diameter of the average subject quite well. The absolute value of the difference between Equations 4.5 and 5.7 is under 2% (Figure 5.2) over the entire range of $[10^{-5}, 10^5]$ blondels (Figure 5.1 right).

$$2.3\ M(D) = 5.2 - 0.45\ ln\left[\frac{\phi}{\bar{\phi}}\right] \tag{5.7}$$

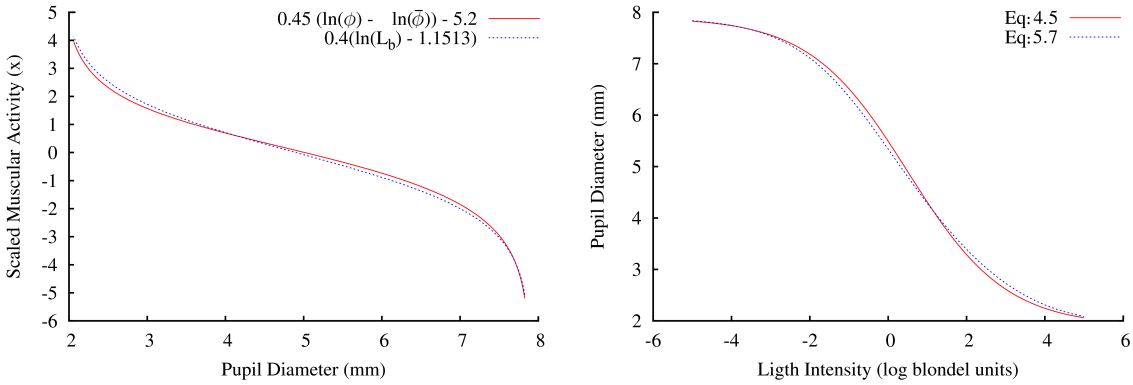

Figure 5.1: High-quality fittings: (left) Both sides of Equation 5.5. (right) Equations 4.5 and 5.7, whose difference in absolute values is under 2% over the entire range $[10^{-5}, 10^{5}]$ blondels.

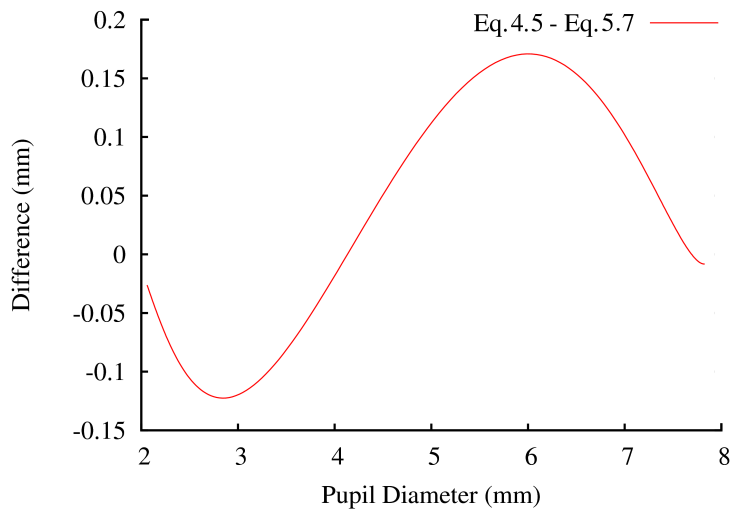

Figure 5.2: Difference between the values predicted by the proposed model and by the Moon and Spencer model. The absolute value of the difference is always less than 2%.

5.2 The Dynamic Case

Equation 5.7 cannot be used to describe the evolution of the pupil diameter in time as a function of instantaneous variations of the light intensity arriving at the pupil. Nevertheless, the obtained constants are still valid for the dynamic case, since the equilibrium is just a special case of the more general pupil behavior, for which the constants should also hold.

In general, one cannot take an equation obtained for the equilibrium and generalize it to the dynamic case. In the proposed model, however, this is possible because of the following constraints:

- $g(A)$ and $M(D)$ have no explicit time dependence;
- The range of values assumed by A (or D) is the same for both the equilibrium and the non-equilibrium cases; and
- There is a one-to-one mapping between A and D.

By introducing time in Equation 5.7, a delay differential equation is obtained that corresponds to the proposed solution for the dynamic case:

$$\frac{dM}{dD}\frac{dD}{dt} + 2.3\ atanh\left(\frac{D-4.9}{3}\right) = 5.2 - 0.45\ ln\left[\frac{\phi(t-\tau)}{\bar{\phi}}\right] \tag{5.8}$$

where D and ϕ are expressed in mm and lumens, respectively. For latency τ, one use Equation 4.1 noting that 1 blondel = 0.0929 fL. Pupil constriction velocity is approximately $3\times$ faster than (re)dilation velocity (ELLIS, 1981; BERGAMIN et al., 1998). This difference is took into account by using different time steps for constriction (dt_c) and dilation (dt_d) in the numerical solver simulation:

$$dt_c = \frac{T_c - T_p}{S} \qquad dt_d = \frac{T_c - T_p}{3S} \tag{5.9}$$

where dt_c and dt_d are measured in milliseconds, T_c and T_p are respectively the current and previous simulation times (times since the simulation started) measured in milliseconds, S is a constant that affects the constriction/dilation velocity and varies among individuals. The higher the S value, the smaller the time step used in the simulation and, consequently, the smaller the pupil constriction/dilation velocity.

Figure 5.3 shows the evolution of the pupil diameter for the Moon and Spencer's average subject simulated using Equation 5.8 considering some abrupt changes in the environment luminance. The results are compared to the static models of Moon and Spencer (Equation 4.5) and of de Groot and Gebhard (1952). Note the smooth variation in pupil diameter and the latency (τ) included in the model.

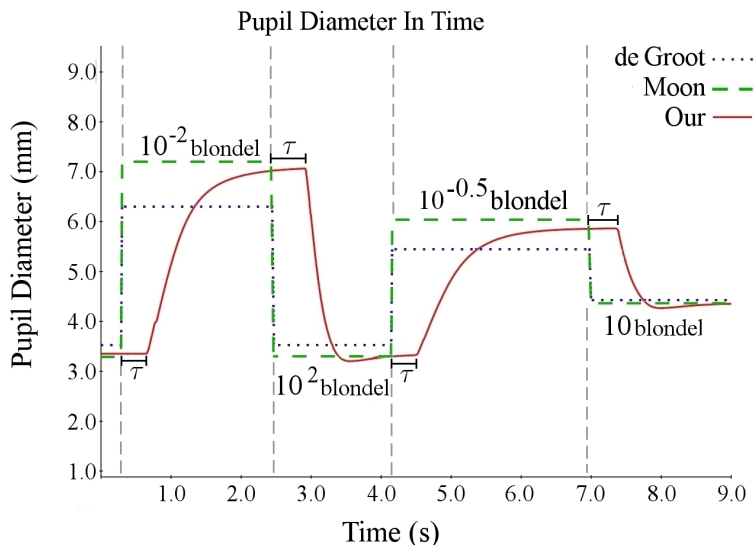

Figure 5.3: Simulated results produced by the proposed model (Equation 5.8) for the average subject of Moon and Spencer under non-equilibrium conditions (solid line). These results are compared to the static models of Moon and Spencer (1944) (dashed line), and of de Groot and Gebhard (1952) (dotted line). Note the latency (τ) predicted by the proposed model and the smooth variation in pupil diameter.

5.3 Solving Delay Differential Equations

Techniques for solving DDEs are well known and several solvers have been implemented using explicit Runge-Kutta methods (SULEIMAN; ISLMAIL, 2001; GUIL-

LOUZIC; HEUREUX; LONGTIN, 1999; PAUL, 1992). However, as the proposed model in this thesis is bounded by finite limits and the pupil diameter is always positive, a simple interactive numerical solution can solve the Equation 5.8 in real time, which is important for interactive applications, such as video games. A linear iterative convergence process was implemented which, given an initial solution and a time step (dT), approximates D by varying dD until $D_t \approx D_{t-1} + dD$. Algorithm 1 shows a pseudocode of the solver applied to Equation 5.8, considering latency as Equation 4.1 and velocities as an approximation to Equations 4.3 and 4.4.

Algorithm 1 Pupil Diameter at Light Intensity

Require: $intensity$ {Light intensity}
Require: $time$ {Time}
Require: $history$ {Initial state in tuples (time,intensity,diameter)}
Require: S {Constant for constriction/dilation velocity}

```
τ ← getLinkAndStarkLatencyFor(intensity) {Equation 4.1}
tuple ← history.get(time − τ)
rightValue ← evaluateRightSideOfEquation5.8(tuple)

dD ← 0
step ← 10;

{100 iterations are enough}
for 0...100 do
    dT ← (time − history.last().time)/S

    if dD > 0 then
        dT ← dT/3 {if dilating decrease the velocity}
    end if

    leftValue ← evaluateLeftSide(dD, dT, diameter)

    if leftValue = rightValue then
        return history.last().diameter + dD
    end if

    if leftValue is not getting closer to rightValue then
        step ← −step/2 {Invert and decrease the size of step}
    end if

    dD ← dD + step
end for

return history.last().diameter {If here, the process did not converge}
```

5.4 Modeling Individual Differences

While Equation 5.8 simulates dynamic pupil behavior, it only does so for the average individual represented by the Moon and Spencer model. There are, however, substantial differences in the way pupils from different individuals react to a given light stimulus. Such variations include differences in diameter (CRAWFORD, 1936; MOON; SPENCER, 1944; GROOT; GEBHARD, 1952; ELLIS, 1981; WINN et al., 1994), latency, and constriction and re-dilation velocities (ELLIS, 1981; BERGAMIN et al., 1998). In order to simulate individual differences, one can not just arbitrarily change the parameter values of the model, as Equation 5.8 may not converge.

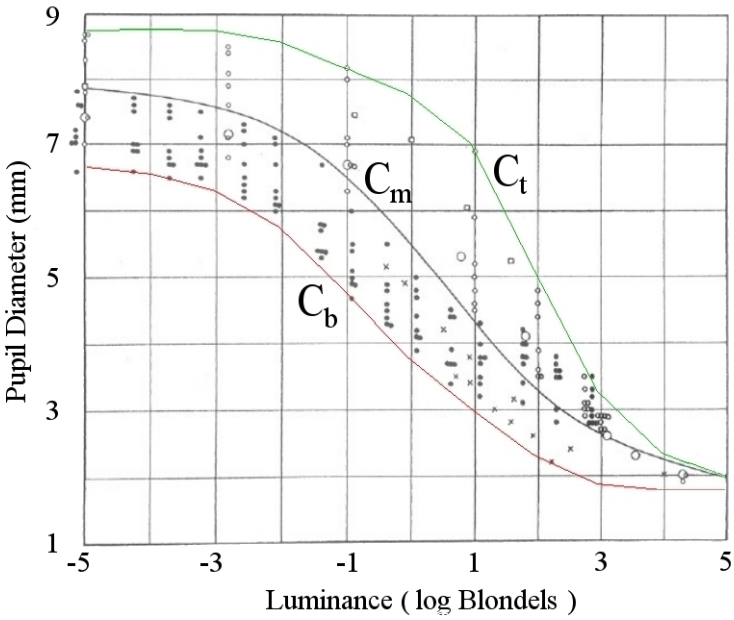

Figure 5.4: Original data used by Moon and Spencer (1944). The curve C_m corresponds to Equation 5.7. The pair of curves C_b and C_t define an envelope containing all data.

Figure 5.4 shows the original data used by Moon and Spencer (1944), with a curve (C_m) corresponding to Equation 5.7. The top and bottom curves, C_t and C_b, respectively, define an envelope containing all pupil diameter values used by Moon and Spencer. C_b, C_m and C_t are treated as isocurves $C(p)$ for some parameter $p \in [0, 1]$, so that $C(0) = C_b$, and $C(1) = C_t$. Individual differences are modeled by associating to each individual I a random number $r_I \in [0, 1]$ that corresponds to an isocurve C_I. C_t and C_b are functions of the pupil diameter:

$$\begin{aligned} C_t(D) &= -0.013D^5 + 0.322D^4 - 3.096D^3 \\ &\quad +13.655D^2 - 25.347D + 18.179 \\ C_b(D) &= -5.442D^5 + 1.387D^4 - 1.343D^3 \\ &\quad +6.219D^2 - 1.317D + 1.219 \end{aligned}$$

To avoid convergence problems and still achieve the results corresponding to isocurve C_I, the final pupil diameter at any time is obtained solving Equation 5.8 for D and then evaluating

$$D_{final} = C_b(D) + (C_t(D) - C_b(D))r_I \tag{5.10}$$

This solution was adopted due to its simplicity and generality: one can easily replace the curves $C_b(D)$ and $C_t(D)$ with new ones, covering new data as they become available, or representing other models (*e.g.*, de Groot and Gebhard (1952)). Since the relative distances of C_m to C_b and C_t vary for different values of D, no value of r_I will exactly recover C_m. This is not a problem, however, as C_m correspond to the average subject. Other parametrization are possible, including ones that interpolate C_m for a given value of the parameter p.

Although the proposed model properly simulates the elastic behavior of the iris muscular activity during changes in lighting conditions, it does not model hippus (*i.e.,* Equation 5.8 will converge to some pupil diameter value if the lighting conditions remain constant). In order to approximate the hippus effect, one can add some small random variations to the light intensity (between $10^{-0.5}$ and $10^{0.5}$ blondels) to induce small variations in the pupil diameter, in the frequency range of 0.05Hz to 0.3Hz (STARK, 1939). This significantly improves the realism of the resulting simulations and animations of indoor scenes. The high luminance usually found in outdoor scenes tend to constrict the pupils and prevent the occurrence of noticeable hippus.

5.5 The PLR Model Validation

In order to validate the proposed model under non-equilibrium conditions, a set of videos were captured from individuals whose eyes present different light sensitivities. The videos were captured with Microsoft Windows Movie Maker using a Cannon ELURA2 miniDV camcorder (NTSC, 720×576 pixels) with progressive scan connected to a PC through a firewire connection. The room's light was kept dimmed, so that the subjects' pupils could naturally dilate to some extent, but not too dark, that the camera could not record the pupil in the individual video frames. Because of these constraints, only the video sequence of two subjects with light eyes were used: one with green eyes and another one with blue eyes. To induce pupil constriction, a small flashlight powered by a single AAA battery (1.5 Volt) was kept at about 20 cm from the subject's right eye. The flashlight was turned on and off several times during the recordings for each subject. The videos were then decomposed into individual frames.

The light intensity was estimated during the on and off states of the flashlight using two frames from each video sequence. These frames were selected from the end portions of the *on* and *off* sequences, so that the pupil's size could be considered in equilibrium. The pupil's diameters were estimated from its number of pixels, assuming an iris diameter of 12 mm. Moon and Spencer's model was inverted to estimate, for each state, the luminance from the pupil diameters of the two subjects. The two luminance results were averaged for each state, obtaining $10^{1.1}$ blondels when the flashlight was on, and $10^{-0.5}$ blondels when the flashlight was off. Given these luminance values and the subjects' corresponding pupil diameters, the Equation 5.10 was used to estimate their corresponding r_I indices, obtaining $r_I = 0.4$ for the green-eye subject and $r_I = 0.03$ for the blue-eye subject. By observing the video sequences, S was set to 500 (Equation 5.9) for the two subjects, as this value made their simulated constriction velocities approximate the ones in the video sequences. The frequency of the light source is setted empirically to $R = 0.4\ Hz$, a value that made the latency estimated by Equation 4.1 approximate the latency observed in the video frames.

Figure 5.5 shows the actual pupil diameter measurements performed on a frame-by-frame basis along 9-second-long sequences captured for each subject. The green '+'

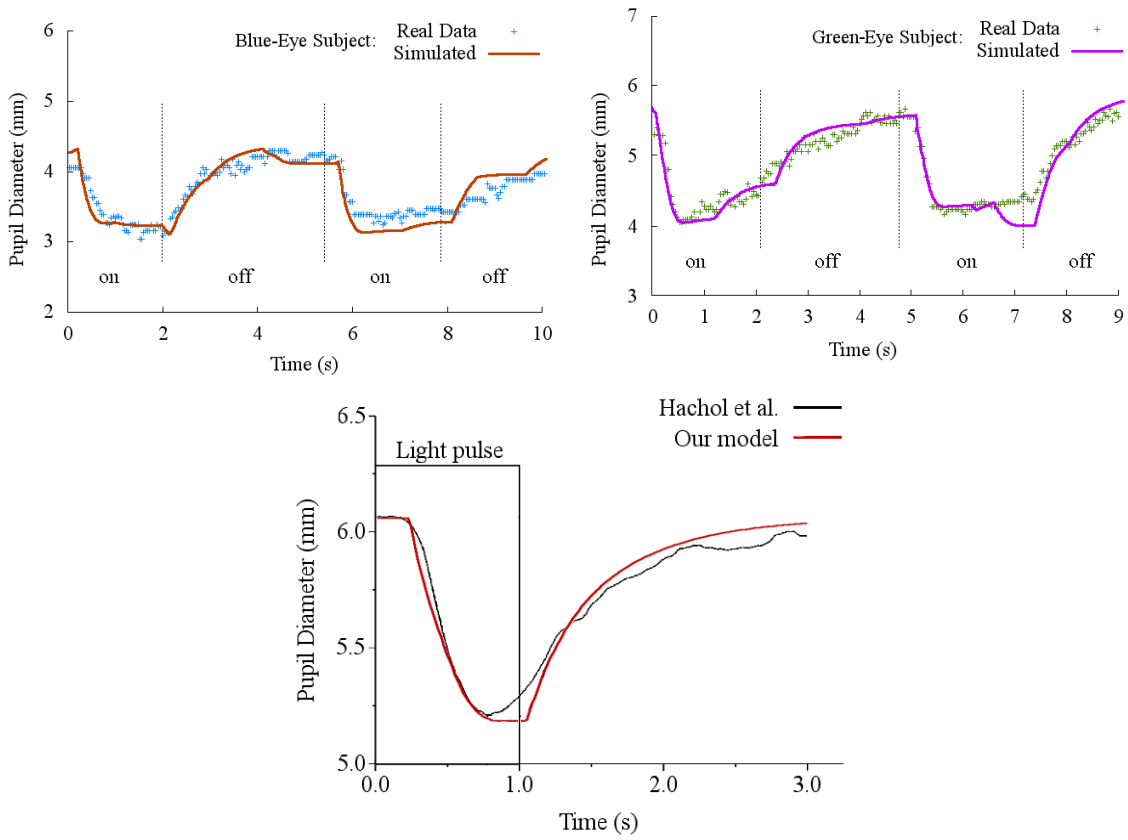

Figure 5.5: Top: Comparison between the simulated results and measurements from real video sequences. The green '+' and the blue 'x' marks represent, respectively, the pupil diameter measurements for the green-eye and for the blue-eye subjects, obtained for all frames along a 9-second-long video sequence. The solid and dashed lines are the pupil diameters predicted by the proposed physiologically-based model for the green-eye and for the blue-eye subjects, respectively. The vertical dotted lines delimit the intervals in which the flashlight was kept on and off for each subject. The predicted values match the actual measurements well. Bottom: Our model (red line) against the Hachol et al. best fitting (black line) (HACHOL et al., 2007).

marks on top represent the measurements for the green-eye subject, while the blue 'x' marks show the measurements of the blue-eye subject. These two subjects illustrate well the inter-subject variability in terms of light sensitivity. The vertical dotted lines delimit the intervals in which the flashlight was kept on and off for each subject. The solid and dashed lines represent the simulated results produced by the proposed model and predict the actual measurements extremely well. These curves were produced automatically from Equation 5.10, on top of which some random hippus effect are added as described in the previous section.

Figure 5.6 (top-left) shows a plot of Equation 5.8 compared with the model of Moon and Spence model as a function of time using velocity and latency models from Link and Stark (Equation 4.1). The highlighted region, inside the circle, shows some behavior predicted by Equation 5.8 that has not been documented in the literature. When the latency (τ) grows from 159.73 ms at 10^2 blondels to 269.04 ms at 10^{-2} blondels, the current time delayed ($t - \tau$) is before of the previous time delayed ($t_{-1} - \tau$) and thus, the current $\phi(t)$ is minor than the previous $\phi(t_{-1})$, while looking only to the s-shaped curve, it should be

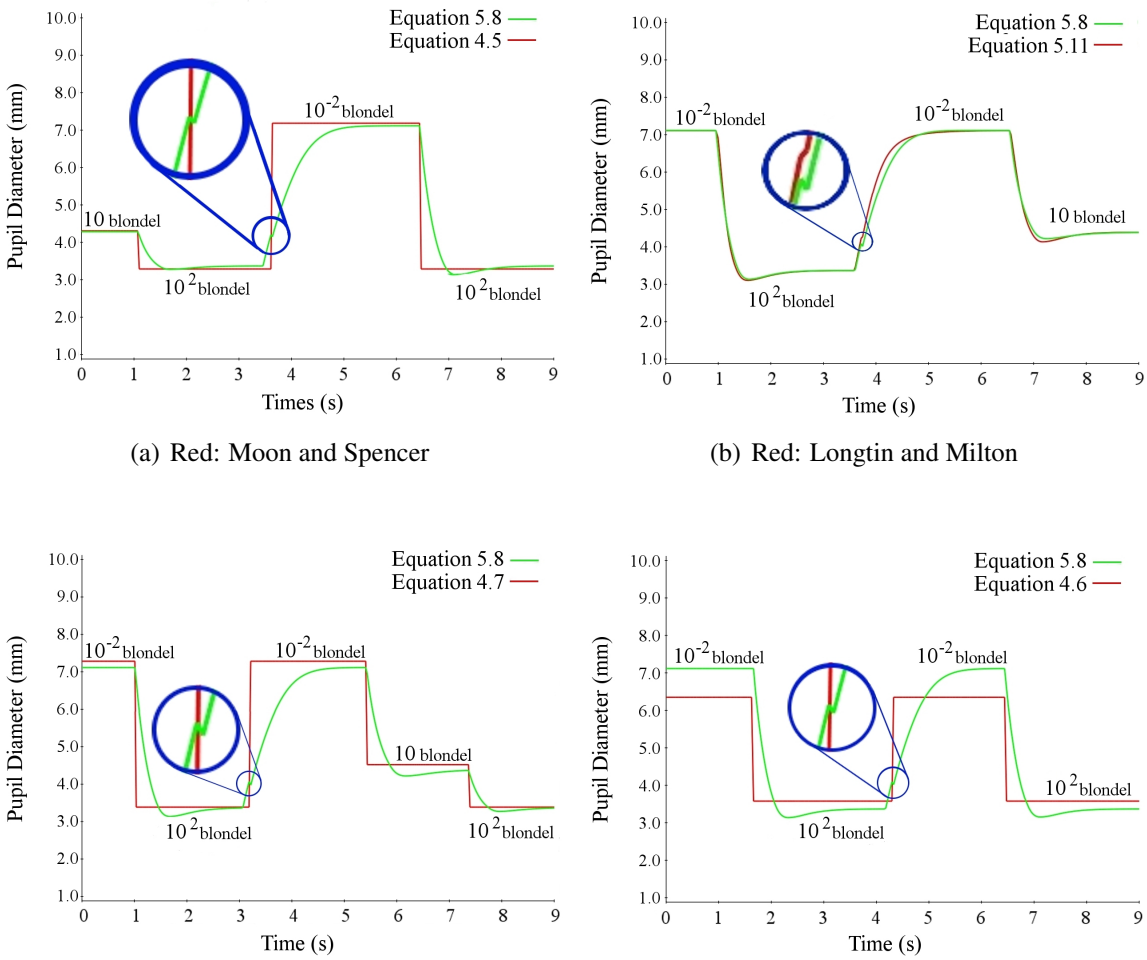

(a) Red: Moon and Spencer

(b) Red: Longtin and Milton

(c) Red: Pokorny and Smith

(d) Red: de Groot and Gebhard

Figure 5.6: Change of pupil diameter as a function of the light intensity for the five models described in this thesis. The green line is always the Equation 5.8 the red line is: (top-left) the original Moon and Spencer model (Equation 4.5); (top-right) the original Longtin and Milton model after the fitting Equation 5.11; (bottom-left) the Pokorny and Smith model (Equation 4.7). (bottom-right) the de Groot and Gebhard model (Equation 4.6). All differential equations are evaluated using the velocity and latency models from Link and Stark (Equation 4.1). The blue circles highlights the change in latency when the light goes off, from 159.73 ms in 10^2 blondels to 269.04 ms in 10^{-2} blondels. This behavior predicted by the proposed model has not been documented in the literature.

greater. In the same way, the DDE solver must converge to a diameter D which is minor than D_{-1}, when it should be greater. This little oscillation in the pupil diameter is created by the Longtin And Milton's model with a non-constant latency and happens every time the latency grows in a difference greater than the solver step.

Figure 5.6 (top-right) shows the pupil diameter in time as a function of the light intensity and compares the results predicted by the model (Equation 5.8) and the Longtin and Milton's model (Equation 4.12) using the Hill function with the following parameters:

$$-2.3\ atanh\left(\frac{D-4.9}{3}\right) \approx -59.2\ +5.84g(A) \tag{5.11}$$

where

$$g(A) = \sqrt[55]{\frac{46.19 * 10^{55}}{A-2.7} - 10^{55}} \tag{5.12}$$

Figures 5.6 (bottom-left) and 5.6 (bottom-right) show comparisons between the proposed model (Equation 5.8) with the models of Pokorny and Smith (Equation 4.7) and de Groot and Gebhard (Equation 4.6). The model of Pokorny and Smith is only a rewrite of Moon and Spencer model.

5.6 Using de Groot and Gebhard Data

The de Groot and Gebhard average subject (Equation 4.6) differs from Moon and Spencer's (Equation 4.5 - Figure 4.2), but one can adapt Equation 5.8 to approximate de Groot and Gebhard's model. In fact, one can map the results of the proposed model to any other. In this case, one first compute the diameter differences between the two empirical models for the light intensity range:

$$D_{diff}(L_b, L_a) = D_{moon}(L_b) - D_{groot}(L_a) \tag{5.13}$$

where D_{moon} is Equation 4.5, D_{groot} is Equation 4.6, L_b is the luminance measured in blondels and L_a the luminance in millilamberts. One then fits a polynomial to the values of D_{diff} and approximates $D_{groot} = D_{moon} - D_{diff}$. From this relation, one gets:

$$\begin{aligned} D_{groot}(D_{moon}) &= D_{moon} \\ &+ 0.0054820\, D_{moon}^5 \\ &- 0.14309\, D_{moon}^4 \\ &+ 1.481\, D_{moon}^3 \\ &- 7.6023\, D_{moon}^2 \\ &+ 19.032\, D_{moon} \\ &- 18.096 \end{aligned} \tag{5.14}$$

The Equation 5.7 is then adapted to approximate Groot and Gebhard's model.

$$2.3\ atanh\left(\frac{D_{groot}(D)-4.9}{3}\right) = 5.2 - 0.45\ ln\left[\frac{\phi(t-\tau)}{\bar{\phi}}\right] \tag{5.15}$$

where $\phi(t) = A(t) * I(t) = area(D(t)) * I(t)$ as $\phi = area(D_{groot}(D(t))) * I(t)$.

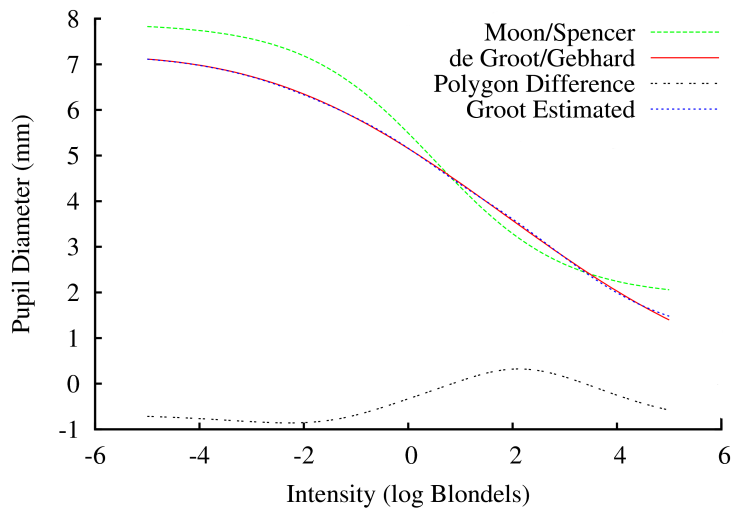

Figure 5.7: The proposed model simulating de Groin and Gebhard data. Models of Moon and Spencer (Green line) and de Groot and Gebhard (Red line), the function difference between them (Brown line), and the evaluation of Equation 5.14 using the converged values from Equation 5.8.

The graph in Figure 5.7 compares the models of Moon and Spencer (green dashed line) and de Groot and Gebhard (red line), The graph also shows the difference between the two models (double dotted brown line), and the evaluation of Equation 5.14 using the diameter from Equation 5.8 in equilibrium (dotted blue line). As one can see, the model was adapted to reach the same pupil diameter of de Groot and Gebhard average subject. Assuming the constraints discussed in Section 5.2, the equation can be extended to the dynamic case:

$$\frac{dM}{dD}\frac{dD}{dt} + 2.3\ atanh\left(\frac{D_{groot}(D) - 4.9}{3}\right) = 5.2 - 0.45\ ln\left[\frac{\phi(t-\tau)}{\bar{\phi}}\right] \tag{5.16}$$

5.7 Summary

This chapter presented the proposed physiological-based time-dependent model for pupil light reflex, showed an extension of the model to support individual differences, hippus, latency and velocity models. The Chapter also discussed a way to implement a DDE solver to the proposed model. The implementation of this model runs in real-time, predicting smooth variation of the pupil diameter under variable lighting conditions. The results of the model were compared with real data, captured from two subjects. The results predicted by the model for the tested subjects were very similar to the observed data. The chapter also discussed a behavior predicted by Longtin and Milton's model that has not been documented in the literature.

6 MODELING THE IRIS DEFORMATION

This chapter describes the second contribution of this thesis: an image-based model for iridal pattern deformation obtained from the analysis of several high-resolution pictures and videos taken from nine volunteers with different induced pupil sizes. A comparison of the model renderings with photographs validates the model.

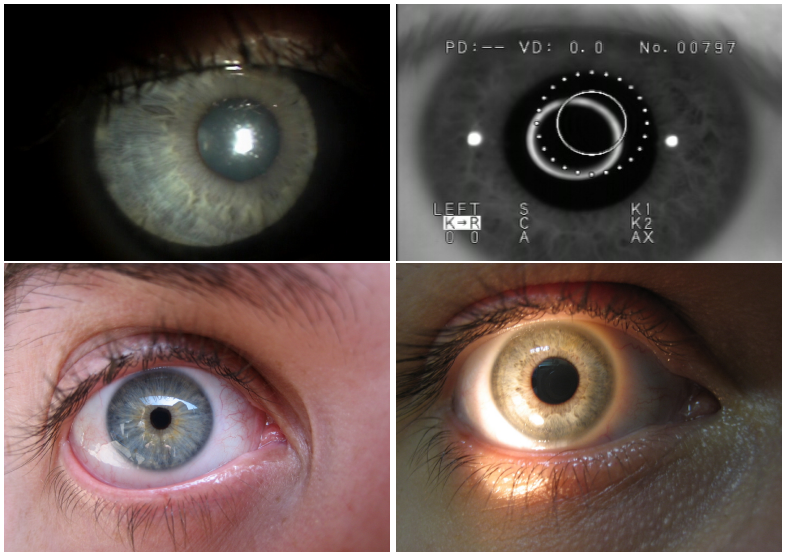

Figure 6.1: (top)Two keratometers images: (top-left) at UFRGS University Hospital and (top-right) at USP/SC Optics Department. (bottom) Photographs of the irises from two subjects.

As the pupil diameter varies, the iridal patterns deform accordingly. In order to produce realist animations of the iris, one needs to simulate such deformations. However, the Biology/Medical literature seems to contain no analytical model describing this process. This thesis derives a model for iridal pattern deformation by analyzing sets of photographs taken from four volunteers under controlled conditions. In the beginning of the work two keratometers were used instead of digital cameras, but their images had limited resolution, were generally out of focus and one of devices could not capture the entire iris surface simultaneously (Figure 6.1 top-left). Images taken with digital cameras can achieve better focus and image resolution, but tend to have more corneal reflection (Figure 6.1 bottom). Nevertheless, the images taken with digital cameras were better suited to track the iris patterns.

In the experiments, an eye doctor dilated the pupils of four volunteers with some mydriatic drug and one person photographed their irises at several stages during the pupil

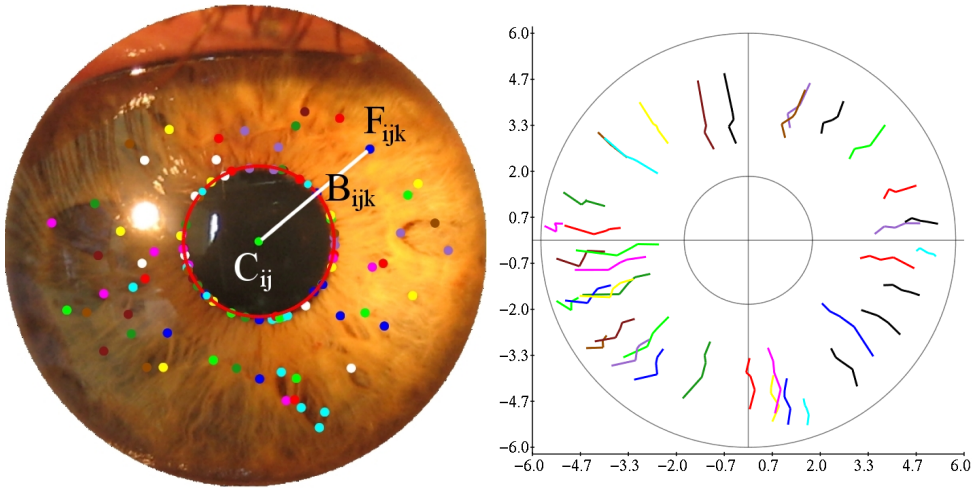

Figure 6.2: Left: Photograph of a volunteer's iris taken during the dilation process. The color dots indicate tracked points F_{ijk}, the center of the pupil C_{ij}, and the border positions B_{ijk} associated with feature points F_{ijk}. A red circle approximates the pupil. Right: Evolution of the positions of the 50 individually tracked iridal features during the dilation process. Each feature is identified by a different color. Note that, for better contrast the color of white dots was changed to black lines.

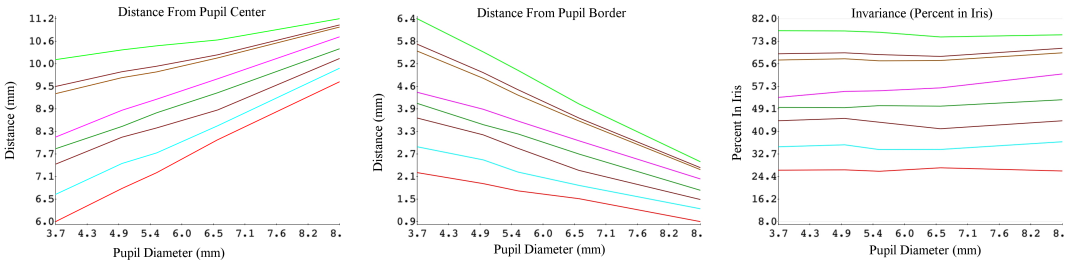

(a) (b) (c)

Figure 6.3: Measured values for some tracked feature points along the dilation process. (a) Distance from F_{ijk} to C_{ij}. (b) Distance from F_{ijk} to the B_{ijk}. (c) Ratio between the distance from F_{ijk} to the B_{ijk} and the local width of the iridal disk. To a first approximation, one can assume that the first two measurements vary linearly, while the third one is constant.

dilatation process using a Canon PowerShot SD 400 camera with macro lens. The images were then cropped to contain only the iris and pupil. The smallest image was 800 $\times$ 800 pixels and the larger ones were rescaled to fit the same dimensions. Thus, let $S_i = \{I_{i1}, I_{i2}, ..., I_{in}\}$ be the set of images from a given volunteer V_i taken along the process sorted by pupil diameter. For each image I_{ij}, a circle on the outer border of the iris and another one at the border of the pupil were positioned (the two circles delimit the iridal disk). The center of the pupil C_{ij} was marked as the center of the inner circle and, after it, a series of iridal features $\{F_{ij1}, F_{ij2}, ..., F_{ijm}\}$ were marked and tracked along the set of images of each volunteer. Since the inner circle is only an approximation to the pupil border and recall that the center of the pupil does not necessarily coincide with the center of the iris, each tracking point F_{ijk} was adjusted the pupil border position B_{ijk} along the segment $F_{ijk} - C_{ij}$. Figure 6.2 (left) shows an image with the tracked features F_{ijk} indicated by a set of colored dots, the approximated pupil border (red circle), and

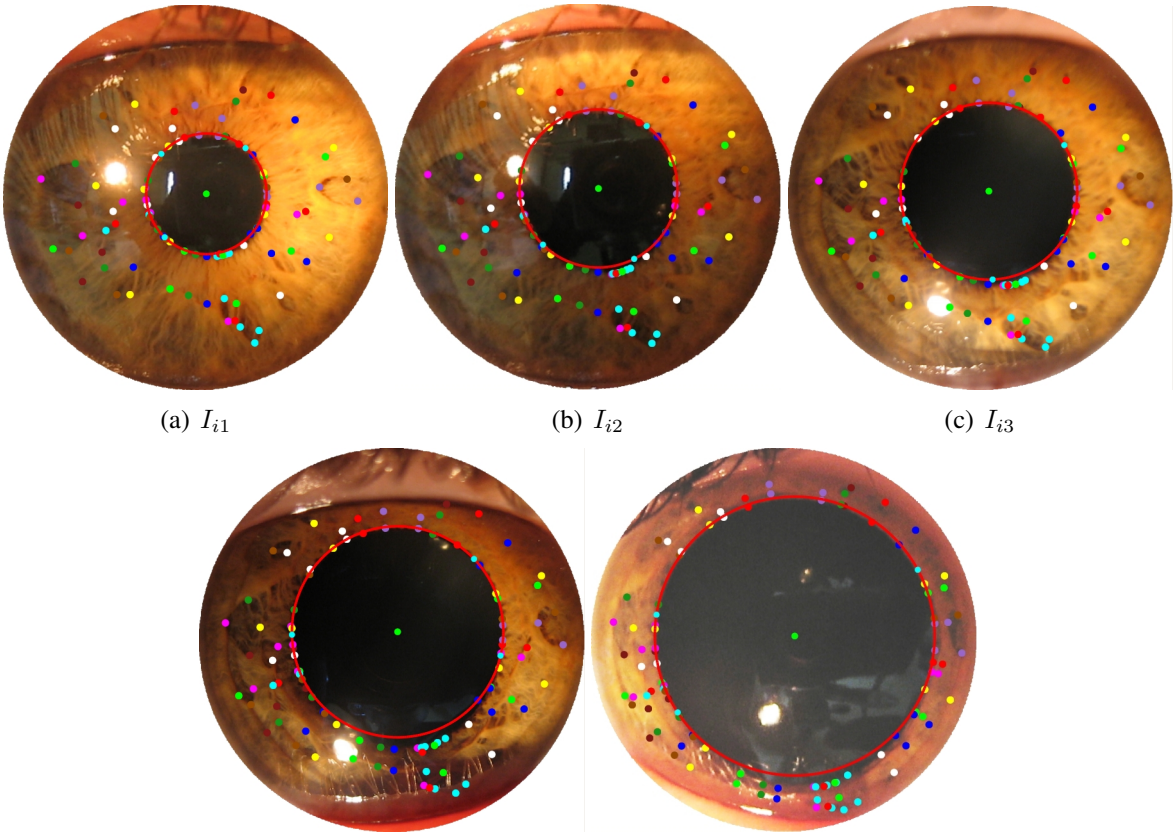

(a) I_{i1} (b) I_{i2} (c) I_{i3}

(d) I_{i4} (e) I_{i5}

Figure 6.4: Set of images used to track the 50 iridal features of one volunteer along the dilation process. Color dots indicate corresponding points in the different images $\{F_{i1k}...F_{i5k}\}$. From left to right, the pupil diameter values are: 3.70, 4.94, 5.53, 6.57, and 8.81 mm, respectively. The apparent changes in iris color are due to the changes in the position of the light source used to illuminate the subject's eye (the camera's flash was turned off).

the actual pupil border position B_{ijk} associated to each feature F_{ijk}. The complete set images used for tracking the features of the iris of this volunteer is shown in Figure 6.4. Figures 6.9 and 6.10 show some of the feature tracked points along the dilation process for two different subjects. In those examples a small number of points was used to facilitate the visual tracking of these points by the reader.

Figure 6.2 (right) shows how the positions of the individually tracked iridal feature points (identified by different colors) changed along the dilation process. The trajectories of the points both on the pupillary and ciliary zones move on approximately radial paths. Although some imprecision in the exact location of the points might have resulted from the manual specification, most of the deviation from the radial paths result from the existence of blood vessels under the iris, and from crypts, and folds (the iris folds its tissue as a result of pupil dilation) (Figure 6.7) that prevent iris points from always moving along radial lines. Such structures vary considerably among individuals but, their influence on the paths of the feature points usually have small magnitude (Figure 6.2 right). Therefore, as a fist approximation, one can assume that the iris points move along straight lines in the radial directions. It is worth noting that Wyatt's 2D model (WYATT, 2000) does not take the influence of these structures into account either. Likewise, points on the pupil-

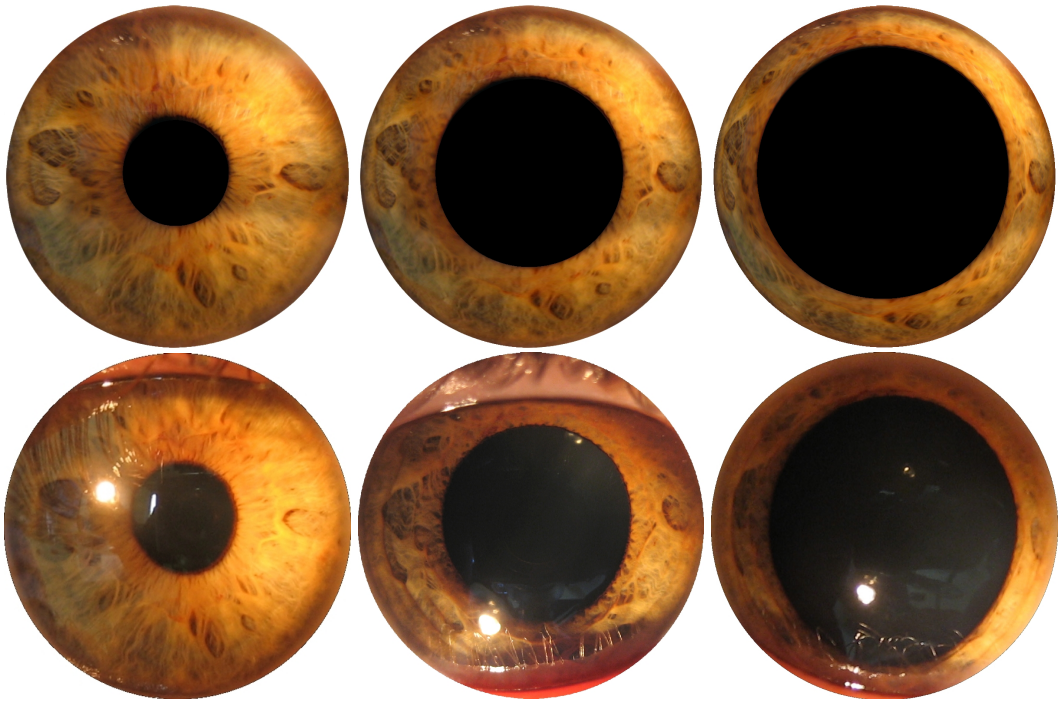

Figure 6.5: Comparison of the results produced by the proposed models with a set of photographs taken from the first subject. Top: renderings produced using the proposed models for environments illuminated with $35,638.70$ and $2,928.78$ lumens/mm^2, respectively, for the first two images. The third one simulates a mydriac-induced dilation. No lighting model was used to render these images. Bottom: photographs of a human iris with the pupil at different diameters.

lary and ciliary zones also move in the same way (along radial lines), characterizing their movement as independent of muscle orientation.

In order to find how fast the feature points F_{ijk} moved, the following measures were computed during the dilation process: (i) the distance from the tracked feature to the pupil center; (ii) the distance from the tracked feature to the pupil border; and (iii) the ratio between the distance from the point to the pupil border and the local width of the iridal disk:

$$r_i = \frac{\|F_{ijk} - B_{ijk}\|}{\|O_{ijk} - B_{ijk}\|} \tag{6.1}$$

where O_{ijk} is a point on the iris outer circle collinear to the segment $F_{ijk} - B_{ijk}$ and $\|.\|$ is the L^2 norm. Then, the following invariance holds for feature point F_{ijk} for all values of pupil diameter. These measurements are plotted in the graphs shown in Figure 6.3. Figure 6.11 shows a comparison between the ratio r_i when the pupil is approximated by a perfect circle (top row) and when Equation 6.1 is used (middle row) for eight group of features.

Discounting the error introduced by the manual specification of the feature points and a little variance made by the influence of certain folds and blood vessels, one can assume the distances defined by (i) and (ii) vary linearly (Figures 6.3a and 6.3b, respectively), while the ratio in (iii) remains constant along the entire dilation process. Figures 6.12 and 6.13 show the graphs discussed in this section for two other volunteers. Figures 6.5 and 6.6 compares the results produced by the proposed models with real photographs.

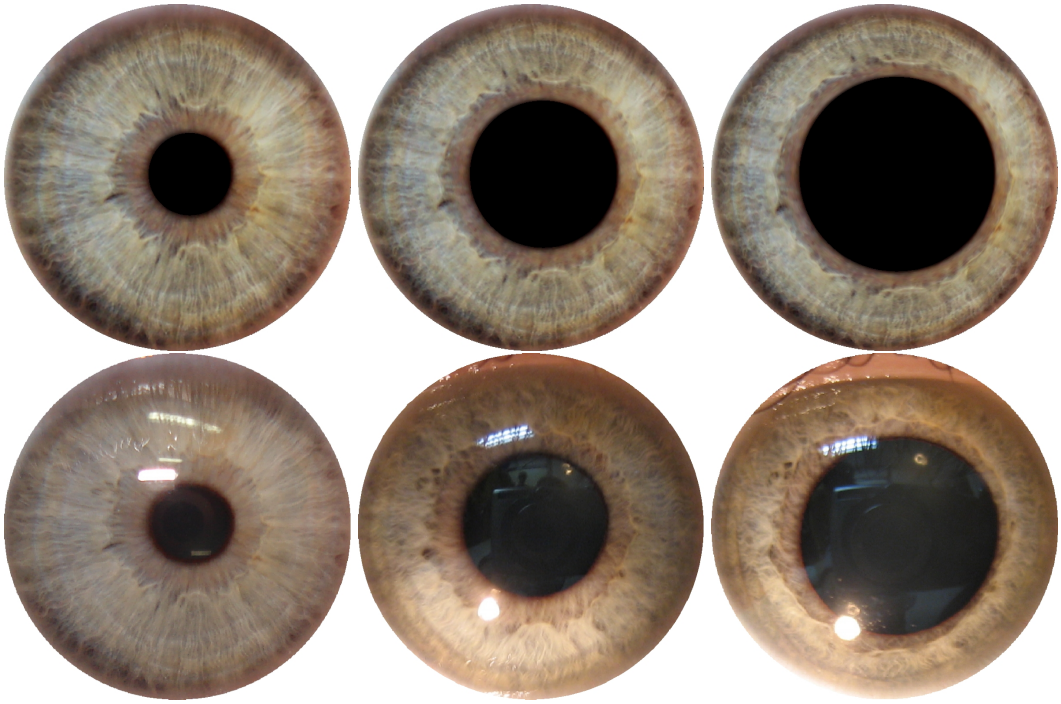

Figure 6.6: Comparison of the results produced by the proposed models with a set of photographs taken from a second subject. Top: renderings produced using the proposed models for environments illuminated with $373,304.70$ and $2,255$ lumens/mm^2, respectively, for the first two images. The third one simulates a mydriac-induced dilation. No lighting model was used to render these images. Bottom: photographs of a human iris with the pupil at different diameters.

Note that the deformed patterns closely approximate the ones in the photographs.

Using high-resolution images of the human iris, we noticed that crypts, pigment spots, and the collarette tend to move in a similar way. Such movements seem to be somehow independent of muscle influences (NEWSOME; LOEWENFELD, 1971), as suggested by Newsome and Loewenfeld. This work also comprove the radial trajectories of the features, however, Newsome and Loewenfeld do not comment some non-radial trajectories which are driven by the position of blood vessels and folds as found here. Some tracked features presents a non-linear behavior, as proposed by Rohen (1951) and formalized in a 2D model by Wyatt (2000). However, this do not always happens and the variations driven by blood vessels and folds are greater than that non-linearity 6.7. Thus, to consider the Wyatt's model and predict the behavior of a specific iris, it is needed first a 3D model for predict the influence of the blood vessels and folds in the iris meshwork. Meanwhile, the approximation to radial trajectories and the constant ratio r_i creates a plausible animation of the iris.

6.1 Animating the Deformed Iridal Patterns

The animation of iridal pattern deformation was using a planar triangle-strip mesh on the disk defined by the two circles delimiting the iris (Figure 6.8 bottom) and using a picture of an iris with a small pupil diameter as a texture. Texture coordinates map the border of the pupil to the inner circle of the mesh, and outer border of the iris to the outer circle of the mesh. Currently, the mesh is tessellated creating a pair of triangles at

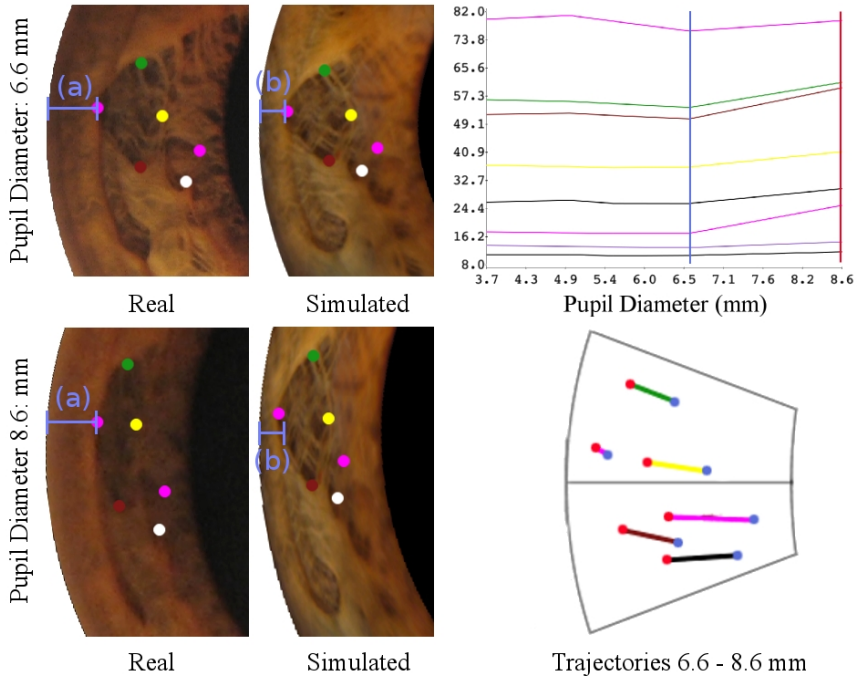

Figure 6.7: Example of the influence of folds in the radial trajectories and in the ratio. Left: real and simulated irises with pupil diameter of $6.6mm$ (top) and $8.6mm$ (bottom); right-top: the ratio r_i for each tracked feature as a function of pupil diameter; right-bottom: the trajectories of the tracked features from $6.6mm$ and $8.6mm$ of pupil diameter; (a) and (b) are the distance from pupil border to the feature in real and simulated irises. Although the (a) remains constant from $6.6mm$ to $8.6mm$, the (b) decreases folowing the image-based model.

every five degrees. The animation proceeds by computing the new pupil diameter D as a function of the incident lighting using Equation 5.10. Each vertex v_i, located on the inner circle of the mesh, is repositioned at a distance $D/2$ along the radial line connecting the center of the pupil to v_i, while keeping their original texture coordinates.

One should recall that the center of the pupil does not necessarily match the center of the iris, thus, it is important to keep the coordinates of the center of the pupil. When the pupil grows, you may also add a variation to the location at the in pupil center up to 20% to the nasal side (FREDDO, 1996).

Figure 6.8(top) shows two renderings created using the proposed model for pupil dilation/constriction and iridal pattern deformation. Note that the patterns deform in a very natural way. These images were simulated for light intensities of 10^5 blondels (left) and 1 blondel (right). The corresponding meshes are shown at the bottom.

Since the implementation of the proposed model uses texture mapping on planar triangle strips, and recalling that François *et al.* (2008) uses a height map to build a 3D mesh of the iris, one can extend the triangle strip by adding the height map to it, whose rendering allows, in close up views, the perception of shadows. This can avoid the distortion of the shadows or light as happens in Figure 6.6 (top). With a three dimensional model for the iris, other extension may support the Lam and Baranoski model (LAM; BARANOSKI, 2006), creating a realistic and predictable iris synthesis and animation.

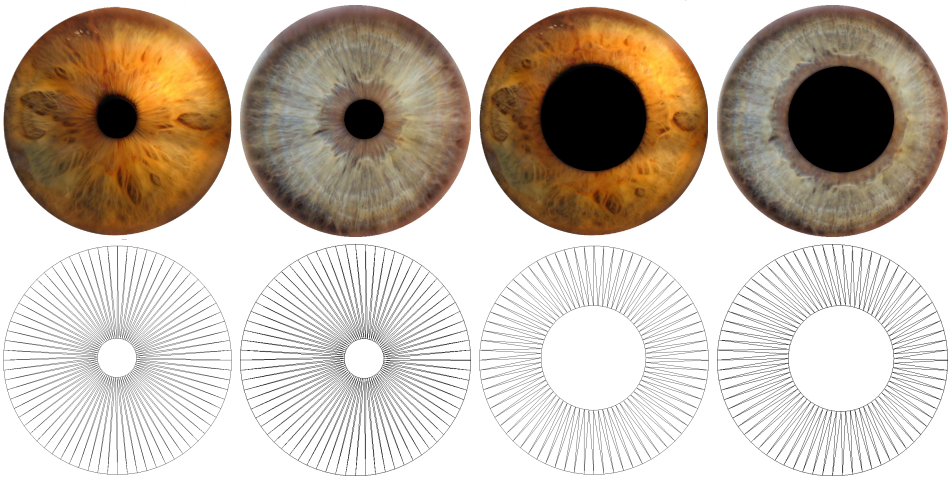

Figure 6.8: Example of irises rendered using the proposed model for pupil dilation/constriction and iridal pattern deformation. Note the natural deformation of the patterns. Top: images simulated for light intensities of 10^5 blondels (left) and 1 blondel (right). Bottom: triangle meshes used for renderings.

6.2 Summary

This Chapter presented an image-based model for iridal pattern deformation. The images generated by the proposed model were compared with photographs taken during light and drug pupil-induced dilation. It also suggested some possibilities for future work supporting the Lam and Baranoski (2006) model and the François *et al.* (2008) 3D rendering technique.

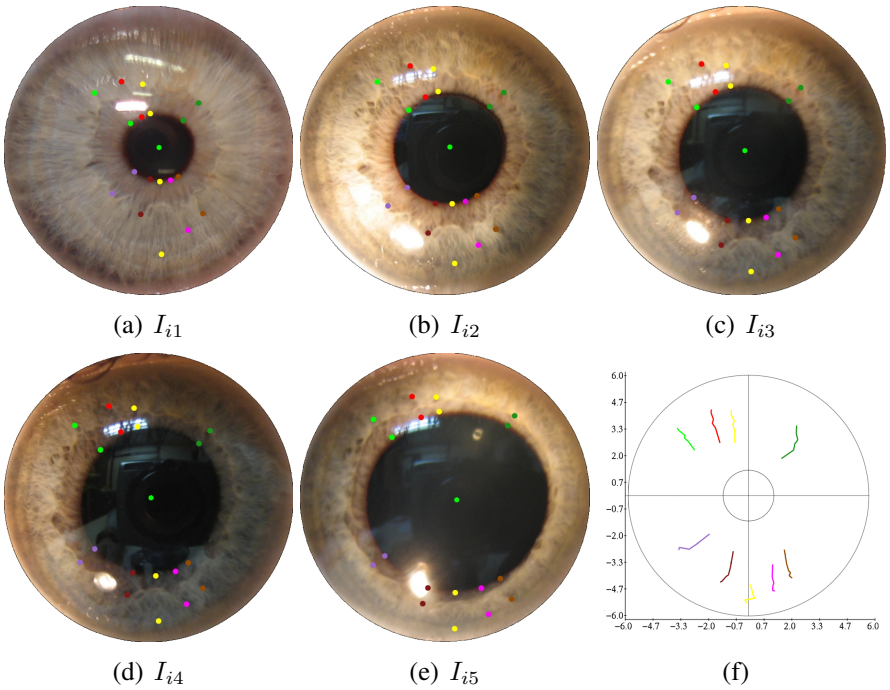

(a) I_{i1} (b) I_{i2} (c) I_{i3}

(d) I_{i4} (e) I_{i5} (f)

Figure 6.9: A subset of the 22 feature points from subject number two tracked along the dilation process: (a) to (e). A plot of the trajectory of these points (f)

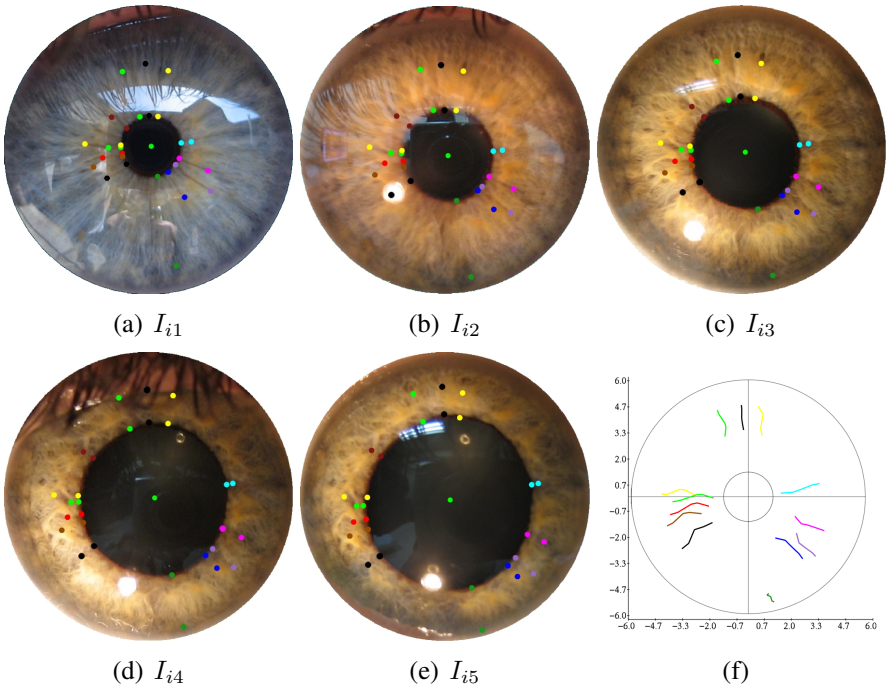

(a) I_{i1} (b) I_{i2} (c) I_{i3}

(d) I_{i4} (e) I_{i5} (f)

Figure 6.10: A subset of the 29 feature points from subject number two tracked along the dilation process: (a) to (e). A plot of the trajectory of these points (f)

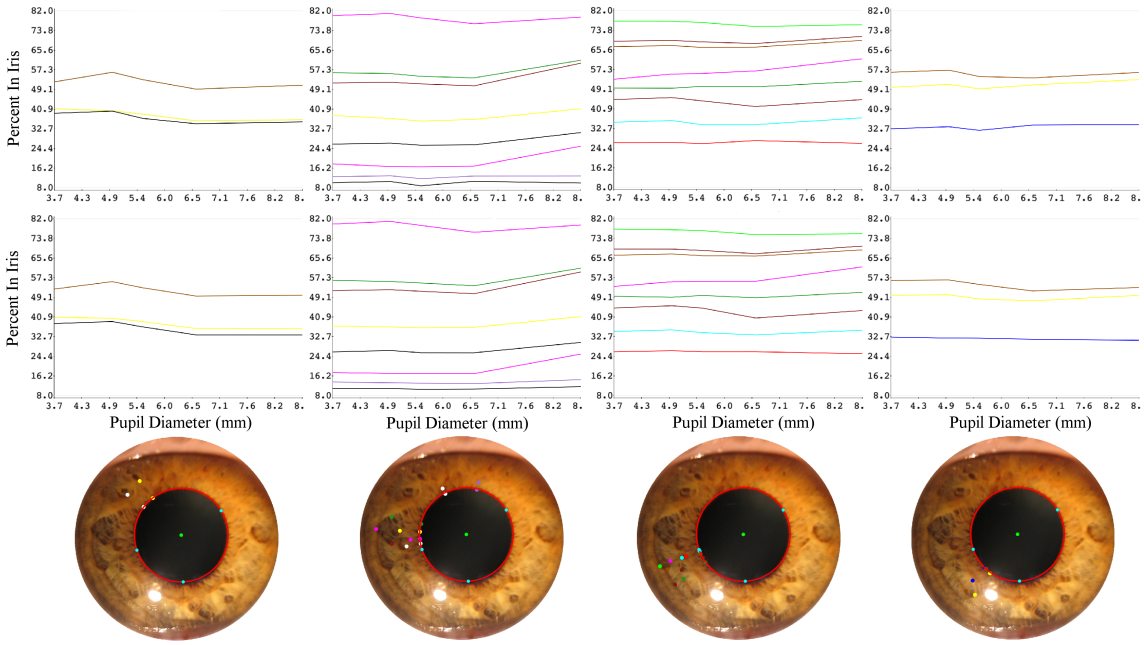

(a) Groups: 1-4

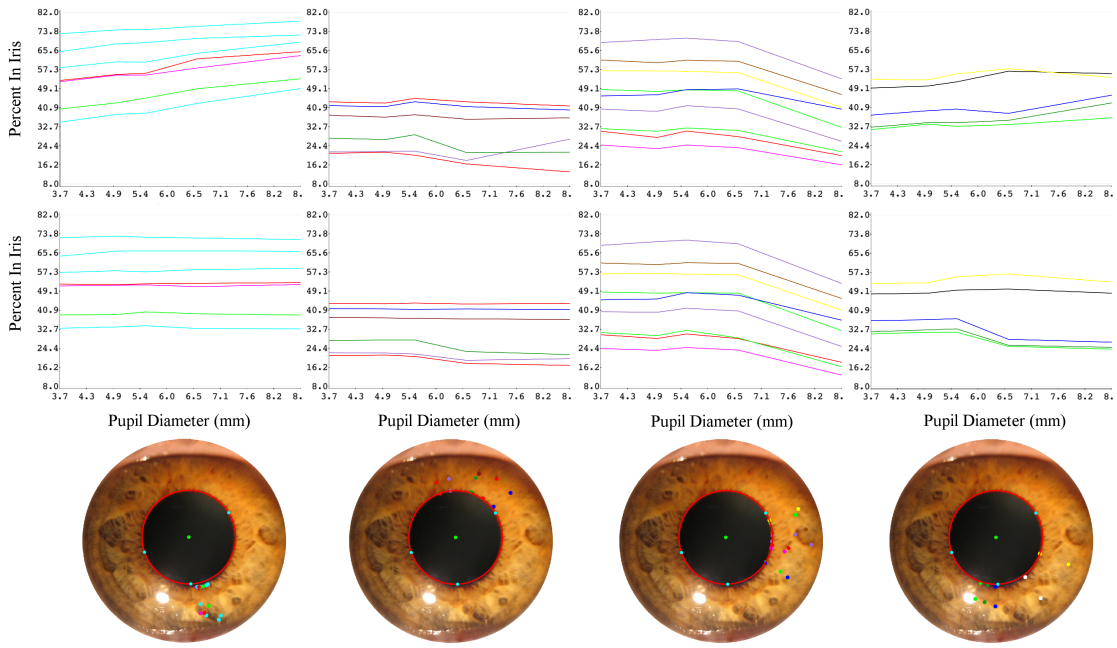

(b) Groups: 5-8

Figure 6.11: The 50 feature points showed in Figure 6.2 divided in eight groups. The top rows of (a) and (b) show the evolution of the ratio between the distance from the feature point to the pupil border, defined by the red circle, and the local width of the iridal disk. The middle rows of (a) and (b) show the same ratio but with the pupil border defined by B_{ijk}. The bottom images show the group of points considered in each column.

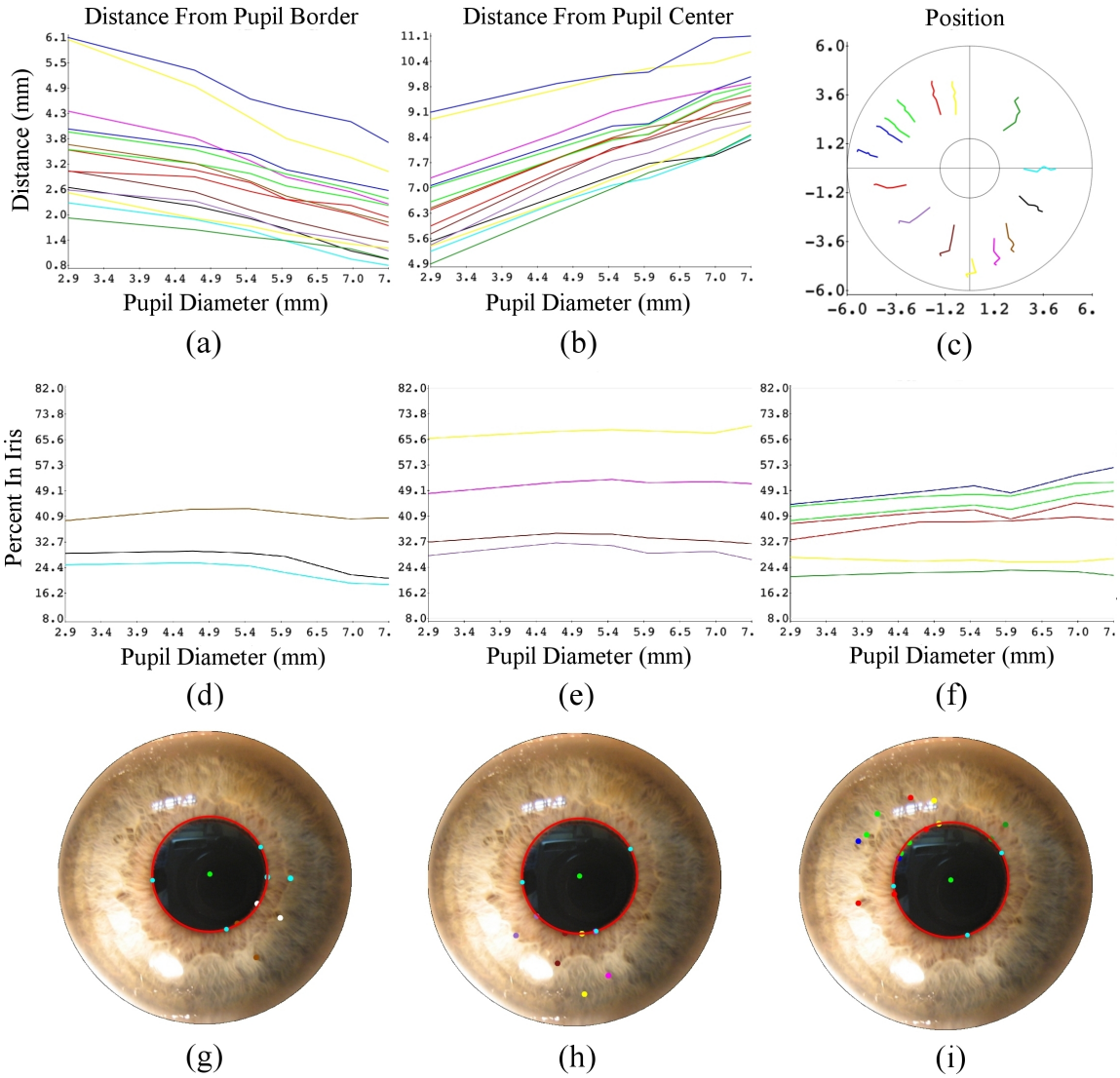

Figure 6.12: Result of the tracked feature points for a second subject. (a) and (b) show the position of each feature F_{ijk} relative to pupil center and pupil border respectively. Note the linearity of these graphs. (c) the trajectories of each feature point when the pupil dilates. (d), (e) and (f) are the ratio r_i (Equation 6.1). Note that, despite some precision problems when marking the features, these ratios are approximately constant.

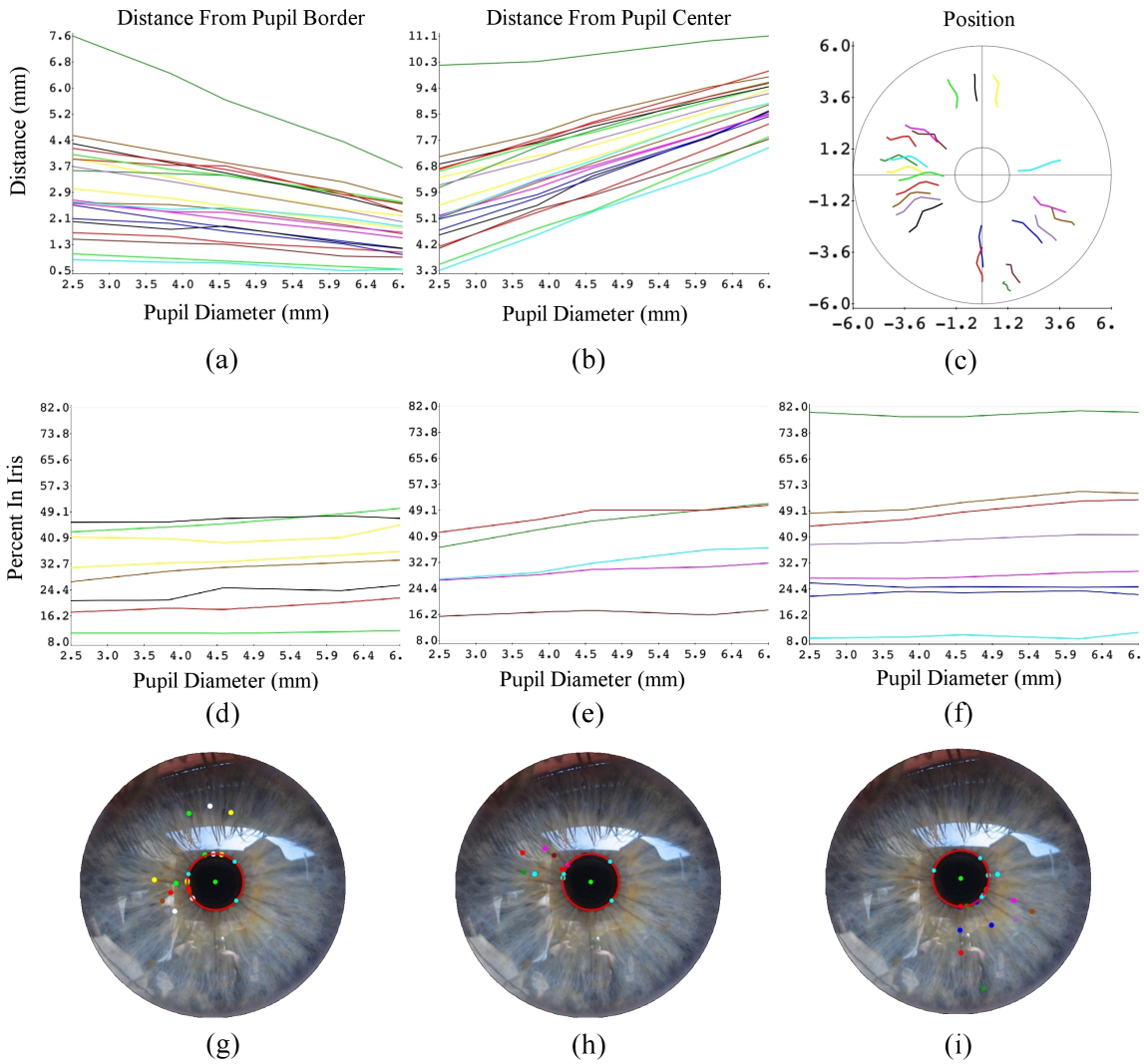

Figure 6.13: Result of the tracked feature points for a third subject. (a) and (b) show the position of each feature F_{ijk} relative to pupil center and pupil border respectively. Note the linearity of these graphs. (c) the trajectories of each feature point when the pupil dilates. (d), (e) and (f) are the ratio r_i (Equation 6.1). Note that, despite some precision problems when marking the features, these ratios are approximately constant.

7 APPLICATION OF THE PROPOSED MODELS IN COMPUTER GRAPHICS

In order to demonstrate the potential use of the proposed models in computer graphics, this thesis presents an application example, which renders a human head model in an environment illuminated by high dynamic range (HDR) light probes. A light probe image is an omnidirectional image that records the incident illumination for each solid angle[1]. An HDR light probe image is a light probe that allows a greater range of exposures than normal digital imaging techniques. The intention of HDR is to accurately represent the wide range of intensity levels found in real scenes recording an scaled value in $lumens/mm^2$. The HDR images were obtained from Paul Debevec's web site (DEBEVEC, 2007) and from ICT Graphics Lab (INSTITUTE OF CREATIVE TECHNOLOGIES, 2007).

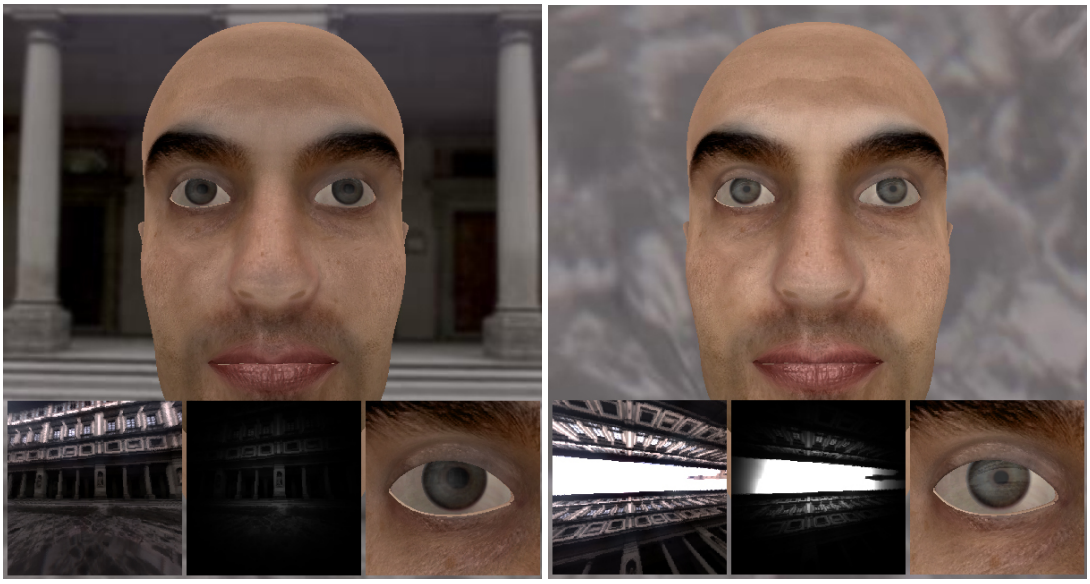

Figure 7.1: Two screenshots from the demo application created to illustrate the use of the proposed models in computer graphics. From left to right, the small images at the bottom show, respectively: the part of the environment seen by the model; an approximation to the image perception on the retina; and a close-up of the eye. Note the differences when looking to a darker place (the building in the left screenshot) and looking to the bright sky (right screenshot).

The head models were obtained from freely available repositories on the net (TURBO SQUID, 2007; BLENDER ARTISTS, 2007) and its original irises were replaced by the

[1]The 3D notion of the 2D angle.

textured triangle-strip as needed by the proposed model. As the head looks at different parts of the environment, its pupil diameters adapt to the irradiance in the solid angle defined by its field of view. This produces interesting animation effects.

Figure 7.1 shows two screenshots of this application. The head model looks at different directions: to the building (Figure 7.1 left) and to the sky (Figure 7.1 right). The small images at the bottom, show, from left to right: (i) the portions of the environment seen by the model; (ii) an approximation to the image perception on the retina and (iii) a close-up view of the model's eyes. Since the distribution of rods and cones in the human retina can be seen as a Gaussian density function with the center at the fovea (HADJIKHANI; TOOTELL, 2000; JONAS; SCHNEIDER; NAUMANN, 1992), in this application, the luminance of the perceived is approximated by modulating the projection of the environment seen by the model (small image at the bottom center of Figure 7.1) using a three-standard-deviation Gaussian filter and summing the luminance of all pixels. Note the changes in pupil size between the two images. The iris on the left was rendered as a perfectly diffuse surface. The rendering on the right includes some Fresnel effect to partially reflect the environment on the cornea surface. Normal maps[2], specular maps[3] and ambient occlusion (BUNNELL, 2005) were also applied to the face. Ambient occlusion is a global shading method that approximates the full global illumination, identifying for each vertex a shadow coefficient. The Lamb Skin effect (nVidia, 2007) was implemented to improve the realism of the skin, since it provides a computationally efficient way to approximate subsurface light scattering effects (Figure 7.2).

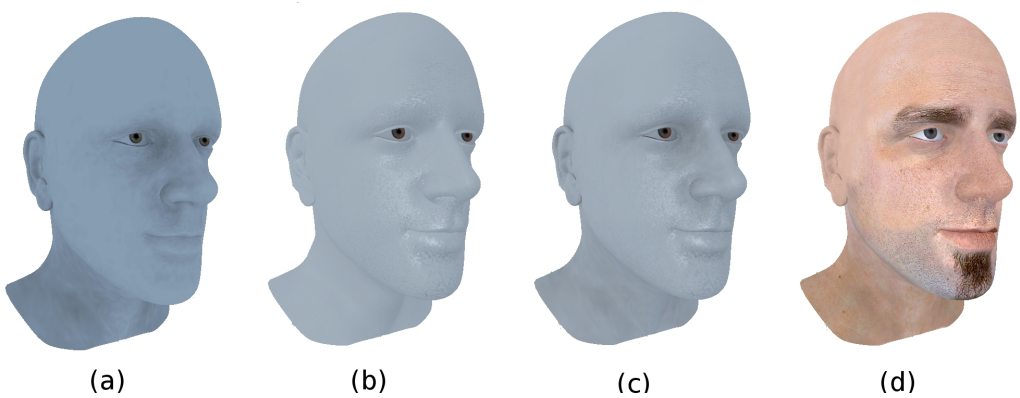

Figure 7.2: Main Effects included in the application to produce realistic effects. (a) Ambient Occlusion (BUNNELL, 2005); (b) Lamb Skin Effect (nVidia, 2007); (c) Lamb Skin Effect plus Ambient Occlusion; (d) Rendering with texture and specular maps.

Unfortunately, the HDR images do not contain the scenes actual luminance values, they are scaled. Thus, in order to produce plausible pupil and iris animations, the stored values are divided by 100.0 and treated the resulting value as lumens per square millimeter. In the future, one can capture HDR images with luminance values in the right scale. This would allow us to compare the animations to real footage obtained in the scene.

[2]Normal maps define the normal for discrete points in a surface

[3]Specular maps record the specular intensity and color of highlights on a surface.

7.1 Summary

This chapter presented an application illustrating the use of the two proposed models to render a 3D model of a human face. An HDR light probe and the models simulate the iridal response to perceived luminance. Many effects were included to produce a more realistic rendering of a human face.

8 CONCLUSION AND FUTURE WORK

This thesis presented new models for realistic renderings of the human iris and pupil light reflex. The proposed physiologically-based model of the pupil light reflex first combines theoretical results from the Mathematical Biology field (LONGTIN; MILTON, 1989) with experimental data collected by several researchers (MOON; SPENCER, 1944), using latency and velocity models from the biological literature. The simplest version of the model is expressed in terms of a non-linear delay-differential equation that describes the changes in the pupil diameter as a function of the environment lighting. As all parameters of the proposed model were derived from experimental data, they correctly simulate the actual behavior of the human iris and pupil from an average subject.

Due to the large variability among individuals, this basic version of the model was extended to include differences, which are modelling as isocurves bounded by the biggest and smallest pupil diameter values found in the original data used by Moon and Spencer (MOON; SPENCER, 1944), along the entire range of luminance values. In order to improve the realism of the resulting simulations, hippus effect is approximate by adding small random variations to the environment light (in the range of 0.05Hz to 0.3Hz (STARK, 1939)). The complete model was validated by comparing the pupil diameters predicted by the model to measurements made on iris video sequences (on a frame by frame basis) for two individuals exhibiting different degrees of light sensitivity.

Other contribution of this work is a study of the iridal pattern deformation as a function of pupil dilation and constriction, as well as an image-based model for realistic animation of such deformations. After an analysis of many high-resolution pictures taken from four volunteers with different induced pupil sizes during an induced pupil-dilation process, we observed that the ratio expressed by Equation 6.1 was approximately constant for all points on iris, and for all tested subjects, independent of the pupil diameter. For rendering purposes, the model of the iris was built as a planar triangle-strip mesh on the disk defined by the two circles delimiting the iris and using a picture of an iris with a small pupil diameter as a texture. The animation moves the mesh points of the pupil border, increasing or decreasing the pupil radius.

In order to demonstrate the potential use of the proposed models in computer graphics, we built an application that renders a human head model in an environment illuminated by HDR light probes. As the head looks at different parts of the environment, its pupil diameters adapt to the irradiance in the solid angle defined by its field of view, producing pleasing animation effects. The proposed models guided by biophysical meaningful parameters produce high-fidelity appearance effects and can be used to produce real-time, predictive and reproducible animations of the pupil and iris under variable lighting conditions and individual differences.

To the best of our knowledge, the proposed PLR model is the first physiologically-

based model for simulating pupil light reflex presented in the graphics literature. It is also the first practical model (*i.e.*, providing actual parameter values) in the literature for simulating the dynamics of pupil and iris under variable lighting conditions, and the first integrated model in all literature to consider individual variability in pupil diameter using general equations for latency, velocity, and an approximation to hippus effect. The proposed image-based model for iridal pattern deformation is the first model of its kind in the graphics literature. The results should find immediate applicability in several areas requiring high-fidelity facial animations, as well as on feature film animations, where the request for increasing levels of realism never ends.

8.1 Discussions and Future Work

For future work, the proposed model could be improved to consider the influence of accommodation and emotional conditions in pupil size. Accommodation and age affect the pupil diameter (WINN et al., 1994) and iris color influences some PLR parameters, such as maximum pupil diameter, latency, and constriction velocity (BERGAMIN et al., 1998). These aspects are currently not taken into account by the proposed model. The main reason is the lack of reliable data over a large range of lighting conditions. For instance, Winn *et al.* (1994) discuss the effect of age on the size of the pupil. Their study, however, only considered luminance values from 10^1 to 10^4 blondels, which corresponds to only about 30% of the luminance range used by the proposed model. Currently, variations in pupil diameters for the same light stimulus were modeled using Equation 5.10, which can approximate the age-related miosis effect reported by Winn *et al.*. Extending the proposed model to handle other phenomena based on biophysical parameters is an interesting direction for future work.

Since, the proposed PLR model was created assuming some uniform light-intensity distribution, it does not consider the light position relative to the viewer. An extension of the model can consider the light position, predicting the Stiles-Crawford effect (i.e. the phenomenon that light reaching the retina after passing near the edge of the pupil is less effective at evoking sensation than light passing through the center of the pupil (STILES; CRAWFORD, 1933)) and observing the distribution of rods and cones in the human retina (HADJIKHANI; TOOTELL, 2000).

HDR light probes record the incident illumination for each solid angle. However, using the representation as proposed by Debevec et al. (2002), it is not possible to retrieve the true luminance value in $lumens/mm^2$ as needed by the PLR model. Thus, a new type of light probe can be defined that stores luminous flux (measured in lumens), which could be used for physically accurate simulations and renditions of PLR using the proposed model.

The current implementation of the proposed iris deformation model uses texture mapping on a planar triangle strip. Such a model can be extended with a height map in a way similar to the technique described in (FRANÇOIS et al., 2008). The rendering of this new model will include support to self-shadowing and view-motion parallax, noticeable in closeup views. Other extension may support the Lam and Baranoski (2006) model, creating a realistic and predictable iris synthesis and animation.

The Longtin and Milton's model and, by inheritance, the proposed PLR model, predicts a small and fast oscillation in pupil diameter when the pupil dilates using the pupil latency as a function of light intensity. This behavior was not documented in the literature and the digital video sequences has no sufficient accuracy to show this oscillation. Some

work will be necessary to verify the actually occurrence of such a predicted behavior. Such a study should probably require the use of specialized equipment, and can be used either to validate this prediction or, otherwise, provide valuable feeback to refine the latency model proposed by Link and Stark (1988) and Ellis (1981) and used as part of our model.

The irises of animals have the same functionality of the human ones. An interesting work could be a validation or adaptation of the iris deformation model against monkeys (CLARKE; ZHANG; GAMLIN, 2003a,b; MAGOUN et al., 1936), cats (HAMMOND; MOUAT, 1985; SCHAEPPI; KOELLA, 1964; MITCHELL, 2006), rabbits (YAMAJI et al., 2003), pigeons (PILAR; VAUGHAN, 1971) or other animals (WEST et al., 1991). This thesis can be used as a guideline to create PLR and iris deformation models for other species.

REFERENCES

BARANOSKI, G. V. G.; LAM, M. W. Y. Qualitative assessment of undetectable melanin distribution in lightly pigmented irides. **Journal of Biomedical Optics**, [S.l.], v.12, n.3, p.030501–1 – 030501–3, May/June 2007.

BELL, A. L. **Histology lab IX**: the eye. Available at: <http://faculty.une.edu/com/abell/histo/histolab3b.htm>. Visited on: Nov. 21, 2007.

BERG, T. J. T. P. V. D.; TAN, K. E. W. P. Light transmittance of the human cornea from 320 to 700 nm for differentages. **Vision Research**, [S.l.], v.34, p.1453–1456, June 1994.

BERGAMIN, O. et al. The influence of iris color on the pupillary light reflex. **Graefes Arch. Clin. Exp. Ophthalmol.**, [S.l.], v.236, n.8, p.567–570, 1998.

BERGAMIN, O.; ZIMMERMAN, M. B.; KARDON, R. H. Pupil light reflex in normal and diseased eyes: diagnosis of visual dysfunction using waveform partitioning. **Ophthalmology**, [S.l.], v.110, n.1, p.106–114, 2003.

BLENDER ARTISTS. **Broken Shadows**: portrait, grunge theme. Available at: <http://blenderartists.org/forum/showthread.php?t=103053>. Visited on: Nov. 21, 2007.

BOETTNER, E. A.; WOLTER, J. R. Transmission of the Ocular Media. **IOVS**, [S.l.], v.1, p.776–783, 1962.

BORES, L. D. **Ocular Anatomy**. Available at: <http://e-sunbear.com/>. Visited on: Nov. 21, 2007.

BUNNELL, M. **GPU Gems 2 - Programming Techniques for High-Performance Graphics and General-Purpose Computation**. [S.l.]: Addison Wesley, 2005. p.223–234.

CALCAGNINI, G. et al. Spontaneous fluctuations of human pupil reflect central autonomic rhythms. **Methods Inf. Med.**, [S.l.], v.39, n.2, p.142–145, June 2000.

CLARKE, R. J.; ZHANG, H.; GAMLIN, P. D. R. Primate Pupillary Light Reflex: receptive field characteristics of pretectal luminance neurons. **J. Neurophysiol.**, [S.l.], v.89, p.3168–3178, 2003.

CLARKE, R. J.; ZHANG, H.; GAMLIN, P. D. R. Characteristics of the Pupillary Light Reflex in the Alert Rhesus Monkey. **J. Neurophysiol.**, [S.l.], v.89, p.3179–3189, 2003.

CRAWFORD, B. H. The integration of the glare effects from a number of glare sources. **Proc. Phys. Soc.**, [S.l.], v.48, n.1, p.35–37, Jan. 1936.

CUI, J. et al. An Iris Image Synthesis Method Based on PCA and Super-Resolution. In: INTERNATIONAL CONFERENCE ON PATTERN RECOGNITION, 2004. **Proceedings...** Washington: IEEE Computer Society, 2004. v.4, p.471–474.

DAUGMAN, J. How Iris Recognition Works. In: INTERNATIONAL CONFERENCE ON IMAGE PROCESSING, 2002. **Proceedings...** [S.l.: s.n.], 2002. v.14, n.1, p.21–30.

DEBEVEC, P. Image-Based Lighting. **IEEE Computer Graphics and Applications**, Los Alamitos, v.22, n.2, p.26–34, Mar./Apr. 2002.

DEBEVEC, P. **Paul Debevec Home Page**. Available at: <http://www.debevec.org/>. Visited on: Nov. 21, 2007.

DECKERT, C. **Eye Design Book**. Available at: <http://www.eyedesignbook.com/index.html>. Visited on: Nov. 21, 2007.

ELLIS, C. J. The pupillary light reflex in normal subjects. **British Journal of Ophthalmology**, [S.l.], v.65, n.11, p.754–759, Nov. 1981.

ESCALOFRIO.FREE.FR. **Fondos de Escritorio Escalofriantes**. Available at: <http://escalofrio.free.fr/fon_orcos/>. Visited on: Nov. 21, 2007.

FERWERDA, J. A. Three Varieties of Realism in Computer Graphics. **Proceedings of SPIE - The International Society for Optical Engineering**, Bellingham, Washington, n.5007, p.290–297, June 2003.

FRANÇOIS, G. et al. Anatomically accurate modeling and rendering of the human eye. In: ACM SIGGRAPH, 2007. **Proceedings...** New York: ACM, 2007. p.59.

FRANÇOIS, G. et al. Subsurface Texture Mapping. **IEEE Computer Graphics and Applications**, [S.l.], v.28, n.1, p.34–42, Jan./Feb. 2008.

FREDDO, T. Ultrastructure of the Iris. **Microscopy Research and Technique**, [S.l.], v.33, p.369–389, 1996.

GLOBO. **Wallpaper Eva Byte**. Available at: <http://www.red-pixel.com.br/images/news/wallpapereva.jpg>. Visited on: Nov. 21, 2007.

GROOT, S. G. de; GEBHARD, J. W. Pupil size as determined by adapting luminance. **J. Opt. Soc. Am.**, [S.l.], v.42, p.492–495, 1952.

GUILLOUZIC, S.; HEUREUX, I. L.; LONGTIN, A. Small delay approximation of stochastic delay differential equations. **Physical Review E**, [S.l.], v.59, n.4, p.3970–3982, 1999.

HACHOL, A. et al. Measurement of pupil reactivity using fast pupillometry. **Physiol. Meas.**, [S.l.], v.28, p.61–72, 2007.

HADJIKHANI, N.; TOOTELL, R. B. H. Projection of Rods and Cones Within Human Visual Cortex. **Human Brain Mapping**, [S.l.], v.1, n.9, p.55–63, 2000.

HAMMOND, P.; MOUAT, G. S. V. The relationship between feline pupil size and luminance. **Experimental Brain Research**, [S.l.], v.59, n.3, p.485–490, 1985.

HESS, E. H.; POLT, J. M. Pupil Size in Relation to Mental Activity during Simple Problem-Solving. **Science**, [S.l.], v.143, p.1190–1192, Mar. 1964.

HILL, A. V. The heat of shortening and the dynamic constants of muscle. **Proc. R. Soc. London B. Biol. Sci.**, [S.l.], v.126, p.136–195, 1938.

HOT WHEELS. **Acceleracers**. Available at: <http://www.hotwheels.com/acceleracers/index.aspx>. Visited on: Nov. 21, 2007.

IMESCH, P.; WALLOW, I.; ALBERT, D. The color of the human eye: a review of morphologic correlates and of some conditions that affect iridial pigmentation. **Surv. Ophthalmol.**, [S.l.], v.41, Suppl. 2, p.177, Feb. 1997.

INSTITUTE OF CREATIVE TECHNOLOGIES. **ICT Graphics Lab**. Available at: <http://gl.ict.usc.edu/>. Visited on: Nov. 21, 2007.

JCH DIGITAL DESIGNS. **Give Your Characters Life**. Available at: <http://www.cocs.com/poser/bestrender2.htm>. Visited on: Nov. 21, 2007.

JONAS, J. B.; SCHNEIDER, U.; NAUMANN, G. O. H. Count and density of human retinal photoreceptors. **Graefe's Archive for Clinical and Experimental Ophthalmology**, [S.l.], v.230, n.6, p.505–510, Oct. 1992.

KASTHURIRANGAN, S.; GLASSER, A. Characteristics of pupil responses during fat-to-near and near-to-far acoomodation. **Ophthal. Physiol. Opt.**, [S.l.], v.25, p.328–339, 2005.

KOJIMA, M. et al. Pupillary light reflex in panic disorder. A trial using audiovisual stimulation. **Eur. Arch. Psychiatry Clin. Neurosci.**, [S.l.], v.254, n.4, p.242–244, 2004.

KRENZ, W. et al. Neurophysiological model of the normal and abnormal human pupil. **IEEE Transactions on Biomedical Engineering**, [S.l.], v.BME-32, n.10, p.817–825, 1985.

LAM, M. W. Y.; BARANOSKI, G. V. G. A Predictive Light Transport Model for the Human Iris. **Computer Graphics Forum**, [S.l.], v.25, n.3, p.359–368, 2006.

LEE, S.; BADLER, J.; BADLER, N. Eyes Alive. **ACM Transactions on Graphics**, [S.l.], v.21, n.3, p.637–644, 2002.

LEFOHN, A. et al. An Ocularist's Approach to Human Iris Synthesis. **IEEE Comput. Graph. Appl.**, Los Alamitos, CA, USA, v.23, n.6, p.70–75, 2003.

LI, Z.; LIANG, P.; SUN, F. Properties of pupillary responses to dynamic random-dot stereograms. **Exp. Brain Res.**, [S.l.], v.168, p.436–440, 2006.

LI, Z.; SUN, F. Pupillary response induced by stereoscopic stimuli. **Exp. Brain Res.**, [S.l.], v.160, p.394–397, 2005.

LINK, N.; STARK, L. Latency of the pupillary response. **IEEE Trans. Bio. Eng.**, [S.l.], v.35, n.3, p.214–218, 1988.

LONGTIN, A.; MILTON, J. G. Modelling autonomous oscilations in the human pupil light reflex using non-linear delay-differential equations. **Bulletin of Math. Bio.**, [S.l.], v.51, n.5, p.605– 624, 1989.

MAGOUN, H. W. et al. The afferent path of the pupillary light reflex in the monkey. **Brain**, [S.l.], v.59, p.234–249, 1936.

MAKTHAL, S.; ROSS, A. Synthesis of Iris Images using Markov Random Fields. In: EUROPEAN SIGNAL PROCESSING CONFERENCE, 2005, Antalya, Turkey. **Proceedings...** [S.l.: s.n.], 2005.

MITCHELL, N. Feline ophthalmology Part 1: examination of the eye. **Irish Veterinary Journal**, [S.l.], v.59, n.3, p.164–168, 2006.

MMVII New Line Productions. **The Lord Of The Rings**. Available at: <http://www.lordoftherings.net/legend/gallery/>. Visited on: Nov. 21, 2007.

MOON, P.; SPENCER, D. On the Stiles-Crawford Effect. **J. Opt. Soc. Am.**, [S.l.], v.34, p.319–329, 1944.

NEWSOME, D.; LOEWENFELD, I. Iris mechanics. II. Influence of pupil size on dynamics of pupillary movements. **Am. J. Ophthalmol.**, [S.l.], v.71, n.1, Part 2, p.353–373, Jan. 1971.

NORBURY, J.; WILSON, R. E. Dynamics of Constrained Differential Delay Equations. **J. Comput. Appl. Math**, [S.l.], v.125, p.201–215, 2000.

nVidia. **Lamb Skin Dusk Effect**. Available at: <http://http.download.nvidia.com/developer/SDK/Individual_Samples/effects.html>. Visited on: Nov. 21, 2007.

nVidia nZone. **NVIDIA Demo**: adrianne. Available at: <http://www.nzone.com/object/nzone_adrianne_home.html>. Visited on: Nov. 21, 2007.

OHTA, N.; ROBERTSON, A. **Colorimetry**: fundamentals and applications. Chichester, England: John Wiley & Sons, 2005. p.1–38.

BROOKS, V.B. (Ed.). **Handbook of Physiology.** Washington: American Physiological Society, 1981. v.2, p.43–106.

PAUL, C. A. H. Developing a delay differential equation solver. **Appl. Numer. Math.**, Amsterdam, The Netherlands, v.9, n.3, p.403–414, 1992.

PEASE, A.; PEASE, B. **The Definitive Book of Body Language**. Rio de Janeiro, RJ, Brasil: Bantam, 2004. v.1, p.103–124.

PILAR, G.; VAUGHAN, P. C. Ultrastructure and Contractures of the Pigeon Iris Striated Muscle. **Journal of Physiology**, [S.l.], v.219, p.253–266, March 1971.

PINGNET, B. et al. Feedback in action: the mechanism of the iris. **Phys. Educ.**, [S.l.], v.23, p.31–35, 1988.

PIXAR. **The Incredibles**. Available at: <http://www.pixar.com/featurefilms/incredibles/>. Visited on: Nov. 21, 2007.

PIXAR. **Finding Nemo**. Available at: <http://www.pixar.com/featurefilms/nemo/>. Visited on: Nov. 21, 2007.

POKORNY, J.; SMITH, V. C. How much light reaches the retina? In: SYMPOSIUM OF THE INTERNATIONAL RESEARCH GROUP ON COLOUR VISION DEFICIENCIES, 13., 1995, Pav, France. **Color Vision Deficiencies XIII: proceedings**, Dordrecht: Kluwer Academic, p.491–511, 1995.

PRIVITERA, C. M.; STARK, L. W. A Binocular Pupil Model for Simulation of Relative Afferent Pupil Defects and the Swinging Flashlight Test. **Bio. Cyber.**, [S.l.], v.94, p.215–224, 2006.

PROENÇA, H. P. M. C. **Towards Non-Cooperative Biometric Iris Recognition.** 2006. Tese (Doutorado em Ciência da Computação) — University of Beira Interior.

REBELANCER. **Rebelance ShrekTW**. Available at: <http://www.rebelancer.com/2005/rebelance_shrektw.jpg>. Visited on: Nov. 21, 2007.

REEVES, P. The response of the average pupil to various intensities of light. **J. Opt. Soc. Am.**, [S.l.], v.4, n.2, p.35–43, Mar. 1920.

ROHEN. Der bau der Regenbogenhaut beim Menschen und einigen Säugern. **Gegenbaur Morphology Journal**, [S.l.], v.91, p.140–181, 1951.

SAGAR, M. et al. A Virtual Environment and Model of the Eye for Surgical Simulation. In: SIGGRAPH CONFERENCE, 1994, Orlando. **Computer Graphics Proceedings...**, New York: ACM, p.205–213, 1994.

SCHACHAR, R. A. Growth patterns of fresh human crystalline lenses measured by in vitro photographic biometry. **Journal of Anatomy**, [S.l.], v.206, p.575, June 2005.

SCHAEPPI, U.; KOELLA, W. P. Innervation of cat iris dilator. **Am. J. Physiol.**, [S.l.], v.207, p.1411–1416, 1964.

SCHMID, R. et al. Effect of Age on the Pupillomotor Field. **Clinical Neural Ophthalmology**, [S.l.], v.24, n.3, p.228–234, Sept. 2004.

SCHOR, C. M.; BHARADWAJ, S. R. A pulse-step model of accommodation dynamics in the aging eye. **Vision Res.**, [S.l.], v.45, n.10, p.1237–1254, May 2005.

SfondiDelDesktop.com. **Images Toon**: a bug s life. Available at: <http://www.sfondideldesktop.com/Images-Toon/A-Bug-S-Life/>. Visited on: Nov. 21, 2007.

STARK, L. W. Stability, Oscillations, and Noise in the Human Pupil Servomechanism. **Proc. of the IRE**, [S.l.], v.47, n.11, p.1925–1939, 1939.

STARK, L. W.; SHERMAN, P. M. A servoanalytic study of consensual pupil reflex to light. **J. Neurophysiol.**, [S.l.], v.20, p.17–26, 1959.

STILES, W. S.; CRAWFORD, B. H. The luminous efficiency of rays entering the eye pupil at different points. **Proc. Roy Soc.**, [S.l.], v.B112, p.428, 1933.

STRAUB, R. H.; THIES, U.; KERP, L. The pupillary light reflex. 1. Age-dependent and age-independent parameters in normal subjects. **Ophthalmologica**, [S.l.], v.204, n.3, p.134–142, 1992.

SULEIMAN, M. B.; ISLMAIL, F. Solving delay differential equations using componentwise partitioning by Runge-Kutta method. **App. Math. and Comp.**, [S.l.], v.122, n.3, p.301–323, 2001.

TAMM, S.; TAMM, E.; ROHEN, J. W. Age-related changes of the human ciliary muscle: a quantitative morphometric study. **Mech. Ageing Dev.**, [S.l.], v.62, n.2, p.209–221, Feb. 1992.

TILMANT, C. et al. Monitoring and Modeling of Pupillary Dynamics. In: ANNUAL INTERNATIONAL CONFERENCE OF IEEE ON ENGINEERING IN MEDICINE AND BIOLOGY SOCIETY, 25., 2003, Cancún, Mexico. **A New Beginning for Human Health**, Piscataway, NJ: IEEE, v.1, p.678–681, 2003.

TREVOR-ROPER, P. D.; CURRAN, P. V. **The Eye and Its Disorders**. Oxford, Boston: Blackwell Scientific Publications; St. Louis, Mo.: Distributors, USA, Blackwell Mosby, 1984. v.3, p.3–75.

TURBO SQUID. **3D max male face head**. Available at: <http://www.turbosquid.com/FullPreview/Index.cfm/ID/357993>. Visited on: Nov. 21, 2007.

TWENTIETH CENTURY FOX. **Ice Age**: the meltdown. Available at: <http://www.iceagemovie.com/>. Visited on: Nov. 21, 2007.

UKAI, K. Spatial pattern as a stimulus to the pupillary system. **J. Opt. Soc. Am. A**, [S.l.], v.2, n.7, p.1094–1100, July 1985.

USUI, S.; STARK., L. A model for nonlinear stochastic behavior of the pupil. **Biological Cybernetics**, [S.l.], v.45, n.1, p.13–21, Aug. 1982.

WATT, A.; WATT, M. **Advanced Animation and Rendering Techniques**. New York: Addison-Wesley, 1992.

WECKER, L.; SAMAVATI, F.; GAVRILOVA, M. Iris Synthesis: a reverse subdivision application. In: COMPUTER GRAPHICS AND INTERACTIVE TECHNIQUES IN AUSTRALASIA AND SOUTH EAST ASIA, 2005, Dunedin, New Zealand. **Proceedings...** New York: ACM, 2005. v.1, p.121–125.

WEI, Z.; TAN, T.; SUN, Z. Nonlinear Iris Deformation Correction Based on Gaussian Model. In: INTERNATIONAL CONFERENCE ON ADVANCES IN BIOMETRICS, ICB, 2007, Soul, Korea. **Advances in Biometrics: proceedings**, Berlin, Springer, p.780–789, 2007. (Lecture Notes in Computer Science, v. 4642).

WERNER, A. Spectral sensitivity of the pupillary system. **Clin. Exp. Optom.**, [S.l.], v.86, n.4, p.235–238, 2003.

WEST, J. A. et al. A comparative study of the anatomy of the iris and ciliary body in aquatic mammals. **Can. J. Zool.**, [S.l.], v.69, n.10, p.2594–2607, 1991.

WIKIPEDIA: the free encyclopedia. **Eye**. Available at: <http://en.wikipedia.org/wiki/Eye>. Visited on: Nov. 21, 2007.

WINN, B. et al. Factors Affecting Light-Adapted Pupil Size in Normal Human Subjects. **IOVS**, [S.l.], v.35, n.3, Mar. 1994.

WYATT, H. J. A minimum-wear-and-tear meshwork for the iris. **Vision Research**, [S.l.], v.40, p.2167–2176, 2000.

WYATT, H. J. **Particular conversation about his meshwork for the iris at Nov. 21, 2007 by e-mail**: <wyatt@sunyopt.edu>. 2007.

YAMAJI, K. et al. Mechanical properties of the rabbit iris smooth muscles. **Vision Res.**, [S.l.], v.43, n.4, p.479–487, Feb. 2003.

YOSHIDA, H. et al. Time-varying properties of respiratory fluctuations in pupil diameter of human eyes. **Methods Inf. Med.**, [S.l.], v.33, n.1, p.46–48, Mar. 1994.

YOSHIDA, H. et al. Statistical properties of simultaneously recorded fluctuations in pupil diameter and heart rate. In: IEEE EMBS, 1995, Montreal: IEEE. **Proceedings...** [S.l.: s.n.], 1995. v.1, p.165–166.

YUAN, X.; SHI, P. A Non-linear Normalization Model for Iris Recognition. In: INTERNATIONAL WORKSHOP ON BIOMETRIC RECOGNITION SYSTEMS, IWBRS, 2005 Beijing, China. **Advances in Biometric Person Authentication**, Berlin: Springer, 2005. (Lecture Notes in Computer Science, v. 3781).

ZUO, J.; SCHMID, N. A. A Model Based, Anatomy Based Method for Synthesizing Iris Images. In: INTERNATIONAL CONFERENCE ON ADVANCES IN BIOMETRICS, ICB, 2006, Hong Kong, China. **Advances in Biometrics: proceedings**, Berlin: Springer, p.428–435, Jan. 2006. (Lecture Notes in Computer Science, v. 3832).

ZUO, J.; SCHMID, N. A.; CHEN, X. On Performance Comparison of Real and Synthetic Iris Images. In: ICIP, 2006. **Proceedings...** [S.l.: s.n.], 2006. p.305–308.

APPENDIX A UNIT CONVERSION TABLE

The Table A.1 shows values to unit conversion of units used in this thesis.

Table A.1: Unit Conversion Table

Value-Unit	.Value	Unit
1.00 candela/square m. [cd/m^2]	3.141592654	blondel
	0.314159265	millilambert [mL]
	0.291863508	foot-Lambert [fL]
1.00 blondel	0.1	millilambert [mL]
	0.09290304	foot-Lambert [fL]
1.00 millilambert [mL]	0.9290304	foot-Lambert [fL]
1.00 lux [lx]	1.00	lumen/square m. [lm/m^2]
1.00 watt/square centimeter [a]	683.00×10^4	lumen/square m. [lm/m^2]
1.00 blondel [b]	10.00×10^{-6}	lumens/square mm. [lm/mm^2]

[a] With a light bulb emitting light at 555 nm

[b] Assuming a perfect diffuse (lambertian) reflector (OHTA; ROBERTSON, 2005)

APPENDIX B MODELOS FOTOREALISTAS PARA DINÂMICA PUPILAR EM FUNÇÃO DA ILUMINAÇÃO E DEFORMAÇÃO DOS PADRÕES DA ÍRIS

Resumo da Dissertação em Português

Animar faces humanas virtuais consiste em imitar uma realidade cheia de detalhes e comum aos nossos olhos. Grande parte da expressão de um personagem é dado por movimentos oculares: sacádico e voluntário; e pelas variações pupilares: contração e dilatação. São estes movimentos que, se realizados de forma coerente, prendem a atenção dos espectadores e transmitem o sentimento desejado pelo autor (LEE; BADLER; BADLER, 2002; WATT; WATT, 1992).

Diferente do resto do corpo, o olho humano e a pupila respondem a estímulos involuntários, que são determinados pelas condições de iluminação, estado emocional e distância focal, entre outras (REEVES, 1920; ELLIS, 1981; CALCAGNINI et al., 2000). O reflexo pupilar em função luz (Pupillary Light Reflex - PLR) é responsável pela contração da pupila em ambientes iluminados e por sua dilatação em ambientes escuros. PLR é uma ação reconhecida, comum aos nossos olhos, e, exceto pela influência de drogas, é o principal fator que determina o tamanho da pupila. Embora que o PLR e as deformações da íris possam ser animadas utilizando técnicas tradicionais de computação gráfica como, por exemplo, representações paramétricas controladas por curvas de velocidade, nós acreditamos que o uso de modelos fisiológicos, guiados por parâmetros com significado físico, possam tornar o processo preditível e automático, criando animações realistas e reprodutíveis.

Neste trabalho nós apresentamos um modelo fisiológico para animação realista do PLR. Nosso modelo combina e estende modelos teóricos (LONGTIN; MILTON, 1989) com dados coletados por vários experimentos relacionando o diâmetro pupilar a intensidade de luz do ambiente (MOON; SPENCER, 1944). Como a íris humana é uma camada muscular fibro-vascular que define padrões que são deformados em função do tamanho da pupila, nós modelamos estas deformações baseando-se em uma análise estatística do comportamento da íris sobre um conjunto de fotografias de íris, em alta resolução, em diferentes níveis de iluminação.

Pelo que pesquisamos, nosso modelo fisiológico para PLR é o primeiro da literatura de computação gráfica, é o primeiro modelo capaz de simular variações individuais em termos de sensibilidade a luz e o primeiro modelo para deformação dos padrões da íris em toda a literatura. Nós demonstramos a eficácia da nossa abordagem comparando os resultados dos nossos modelos contra fotografias e vídeos capturados de iris humanas.

B.1 Modelos Existentes Para PLR

A pupilometria descreve modelos, construídos a partir de experimentos e um conjunto de medidas discretas, que relacionam diretamente a iluminação que atinge a retina com um tamanho médio da pupila entre indivíduos (MOON; SPENCER, 1944; GROOT; GEBHARD, 1952; POKORNY; SMITH, 1995). As medidas são tomadas quando a pupila está estável, após uma alteração de iluminação. Estes modelos são, até onde sabemos, todos atemporais, portanto não descrevem o comportamento fora do estado de equilíbrio. De todos eles, o modelo mais popular é o de Moon e Spencer, que é dado por:

$$D = 4.9 - 3tanh\left[0.4(log_{10}(L_b) - 0.5)\right] \tag{B.1}$$

onde o diâmetro pupilar D varia de 2 a 8mm, e L_b é o nível de luminância do ambiente expressa em blondels e variando de 10^5 blondels em dias ensolarados até 10^{-5} blondels em noites escuras.

Modelos para PLR, baseados em observações anatômicas e fisiológicas, foram criados para expressar o relacionamento entre as diversas estruturas do corpo humano envolvidas no processo, sem considerar dados experimentais. Longtin e Milton (1989) definiram um modelo teórico para o caminho neural entre o estímulo de luz recebido pela pupila até a ação de contração ou dilatação da íris:

$$\frac{dg}{dA}\frac{dA}{dt} + \alpha g(A) = \gamma\, ln\left[\frac{\phi(t-\tau)}{\bar{\phi}}\right] \tag{B.2}$$

onde

$$g(A) = \sqrt[n]{\frac{\Lambda\theta^n}{A-\Lambda'} - \theta^n} \tag{B.3}$$

e Λ' e $\Lambda + \Lambda'$ são respectivamente áreas mínima e máxima para a pupila, θ é o valor para a atividade muscular onde a pupila possui tamanho médio, α uma taxa constante, γ é um fator de proporcionalidade, t é o tempo, τ é a latência entre o momento do estímulo e a resposta da íris, ϕ é o nível de luz na retina medida em lumens e definido como $\phi = IA$, onde I é a iluminância em lumens/mm^2 e A é a área da pupila em mm^2 e $\bar{\phi}$ é um limite inferior para o nível de luz na retina (o nível de luz no qual variações abaixo dele não mudam a área pupilar). $g(A)$ é apenas uma função com um intervalo pré-definido no conjunto imagem e que simula as propriedades elasto-mecânicas dos músculos em geral.

Note que, embora este modelo seja temporal, as constantes não representam unidades físicas. Por exemplo, θ é definido sobre uma unidade não conhecida e, portanto não pode ser medida, chamada atividade muscular. Valores incorretos para estas constantes podem criar comportamentos não realistas e não convergir para uma solução.

B.2 Proposta de modelo para PLR

Nosso modelo une o modelo teórico e temporal de Longtin e Milton (Equation B.2) e o modelo experimental e estático de Moon e Spencer (Equation B.1).

Sob condições de iluminação constante, a área pupilar no modelo de Longtin e Milton convergirá para um estado de equilíbrio, onde:

$$\frac{dg}{dA}\frac{dA}{dt} = 0$$

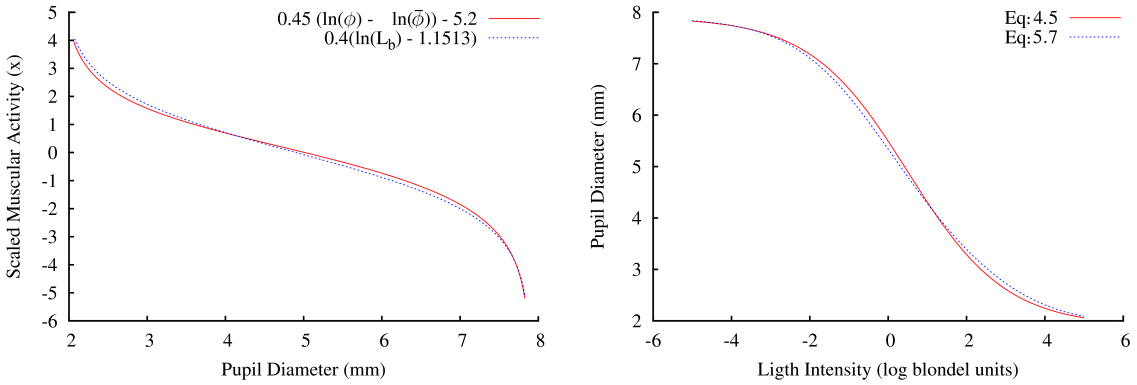

Figura B.1: Qualidade dos Fittings: (esquerda) Ambos os lados da equação B.8. (direita) Equações B.1 e B.10, na qual a diferença em valores absolutos é menor que 2% sob o intervalo $[10^{-5}, 10^{5}]$ blondels.

Sob esta circunstância e assumindo que não há ocorrência de hippus, ϕ torna-se independente de tempo. Manipulando algebricamente os modelos, podemos reescrevê-los para as equações abaixo:

$$\alpha g(A) = \gamma\,(ln(\phi) - ln(\bar{\phi})) \tag{B.4}$$

$$-2.3\ atanh\left(\frac{D-4.9}{3}\right) = 0.4(ln(L_b) - 1.1513) \tag{B.5}$$

onde $atanh$ é o arco-tangente hiperbólico. Note a semelhança no formato das equações. Para que a Equação B.4 apresente valores de área pupilar comparáveis ao diâmetro pupilar pela Equação B.5, sob as mesmas condições de iluminação, tem-se:

$$-2.3\ atanh\left(\frac{D-4.9}{3}\right) \approx \alpha g(A) \tag{B.6}$$

$$0.4(ln(L_b) - 1.1513) \approx \gamma(ln(\phi) - ln(\bar{\phi})) \tag{B.7}$$

Após um fitting das duas equações, obtivemos:

$$0.4(ln(L_b) - 1.1513) \approx 0.45\ (ln(\phi) - ln(4.8118\ \times\ 10^{-10})) - 5.2 \tag{B.8}$$

A figura Figura B.1(esquerda) mostra a qualidade da aproximação. Dada a Equação B.6, podemos substituir $\alpha g(A)$ por $M(D)$ e utilizar os valores das constantes do lado esquerdo da Equação B.8 na Equação B.4. O modelo que prediz o diâmetro pupilar em condições de iluminação estável é:

$$M(D) = atanh\left(\frac{D-4.9}{3}\right) \tag{B.9}$$

$$2.3\ M(D) = 5.2 - 0.45\ ln\left[\frac{\phi}{4.8118\ \times\ 10^{-10}}\right] \tag{B.10}$$

Voltando a considerar o modelo temporal, podemos efetuar a mesma troca da função atemporal $g(a)$ pela $M(D)$ e utilizar os mesmos valores para as constantes. Desta forma, o nosso modelo dinâmico é:

$$\frac{dM}{dD}\frac{dD}{dt} + 2.3\ atanh\left(\frac{D-4.9}{3}\right) = 5.2 - 0.45\ ln\left[\frac{\phi(t-\tau)}{4.8118\ \times\ 10^{-10}}\right] \tag{B.11}$$

onde D e ϕ são expressados em mm e lumens, respectivamente. Para latência τ, nós utilizamos o modelo de Link e Stark (1988).

Como velocidade de contração é aproximadamente $3\times$ mais rápida do que a velocidade de (re)dilatação (ELLIS, 1981; BERGAMIN et al., 1998), nós aplicamos esta diferença no tamanho do passo da simulação numérica que resolve o modelo:

$$dt_c = \frac{T_{ms} - T_{ms}^{-1}}{S} \qquad dt_d = \frac{T_{ms} - T_{ms}^{-1}}{3S} \tag{B.12}$$

one dt_c e dt_d são medidos em millisegundos, T_{ms} e T_{ms}^{-1} são, respectivamente, os tempo de simulação atual e anterior medido em millisegundos. S é uma constante que afeta as velocidades no sentido de simular variações individuais.

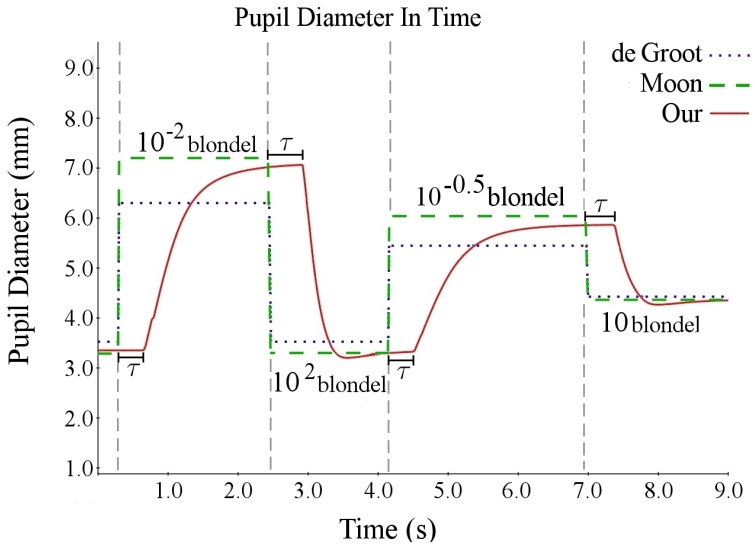

Figura B.2: Resultados da simulação utilizando nosso modelo (Equação B.11) para o indivíduo médio de Moon e Spencer sobre condições de iluminação variáveis (linha sólida). Estes resultados são comparados com os modelos estáticos de Moon e Spencer (1944) (linha tracejada), e de Groot e Gebhard (1952) (linha pontilhada). Note a latência em nosso modelo.

Figura B.2 mostra a evolução do diâmetro pupilar para um indivíduo médio de Moon e Spencer. O Gráfico compara a Equação B.11 com a Equação B.1.

Embora que a Equação B.11 simule o comportamento de um indivíduo médio representando pela curva de Moon e Spencer, existem variações entre indivíduos relacionadas aos seguintes parâmetros: latência (CRAWFORD, 1936; MOON; SPENCER, 1944; GROOT; GEBHARD, 1952; ELLIS, 1981), velocidade de contração e (re)dilatação (ELLIS, 1981; BERGAMIN et al., 1998), idade (WINN et al., 1994) entre outros. Para estimar estas diferenças individuais nós criamos um intervalo de variação dado por curvas de diâmetro pupilar máximo e mínimo baseado nos dados de Moon e Spencer, como mostrado na Figura B.3. A partir desta informação, cria-se iso-curvas C_I entre os limites máximo e mínimo. O diâmetro pupilar final é definido resolvendo a Equação 5.8 e submetendo o diâmetro encontrado na equação B.13

$$D_{final} = C_b(D) + (C_t(D) - C_b(D))r_I \tag{B.13}$$

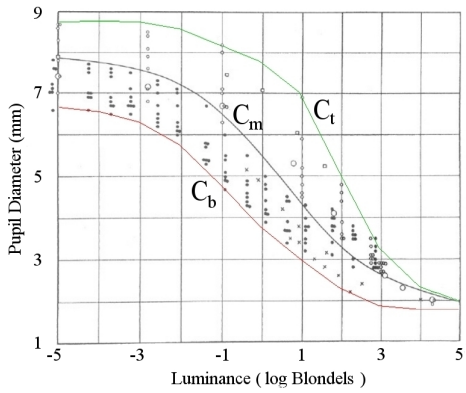

Figura B.3: Dados originais de Moon e Spencer (1944). A curva C_m corresponde a Equação 5.7. O par de curvas C_b e C_t definem um envelope contendo a faixa de diâmetro pupilar disponível para cada intensidade de luz.

Para modelar a Hippus, pequenas variações pupilares que ocorrem mesmo com uma intensidade de luz estável, adiciona-se pequenas variações na intensidade de luz na faixa de $10^{-0.5}$ e $10^{0.5}$ blondels e na freqüência de 0.05Hz a 0.3Hz (STARK, 1939). Estas variações melhoram consideravelmente o realismo das cenas. Validamos o modelo em comparações com dados reais, como mostrado na Figura B.4.

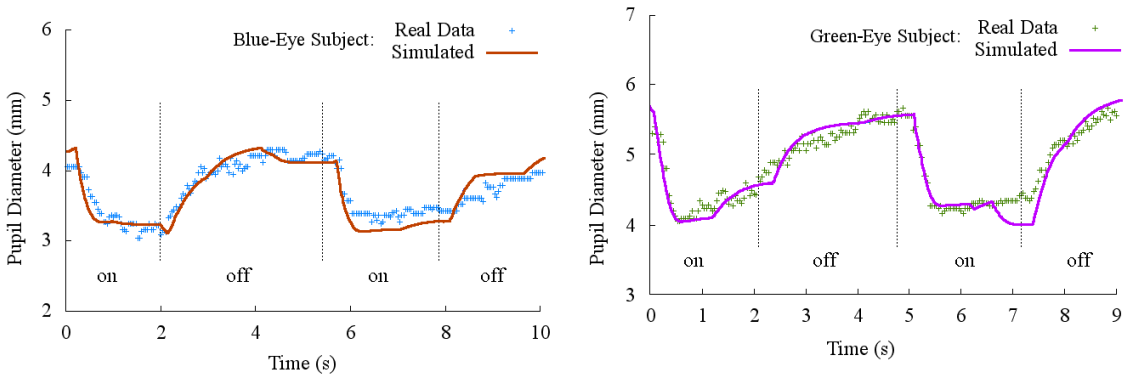

Figura B.4: Cima: Comparação entre os resultados simulados e medidas a partir de dados reais. O '+' verde e o 'x' azul representam, respectivamente, o diâmetro pupilar medido a partir da captura de duas seqüências de vídeos com dois indívidiuos: um de íris verdes e outro de íris azuis. As linhas sólidas e tracejadas representam o diâmetro pupilar calculado pelo nosso modelo. As linhas verticais delimitam os intervalos de luz ligada e desligada.

B.3 Modelo Para Deformação dos Padrões da Íris

O modelo para deformação dos padrões da íris, proposto neste trabalho, foi criado a partir de um conjunto de fotos capturadas durante um processo de dilatação pupilar induzido. As melhores fotos foram separadas, ordenadas pelo tamanho da pupila e as características mais salientes das íris foram marcadas manualmente. A Figura B.5 mostra

um subconjunto dos pontos analisados. Note que os padrões movem-se radialmente e, desconsiderando as perturbações provocadas pela estrutura da íris do indivíduo, o comportamento de cada saliência pode ser aproximado por uma linha reta radial. Além disso as saliências permanecem em suas posições relativas a largura da pupila, caracterizando uma constância que define o nosso modelo.

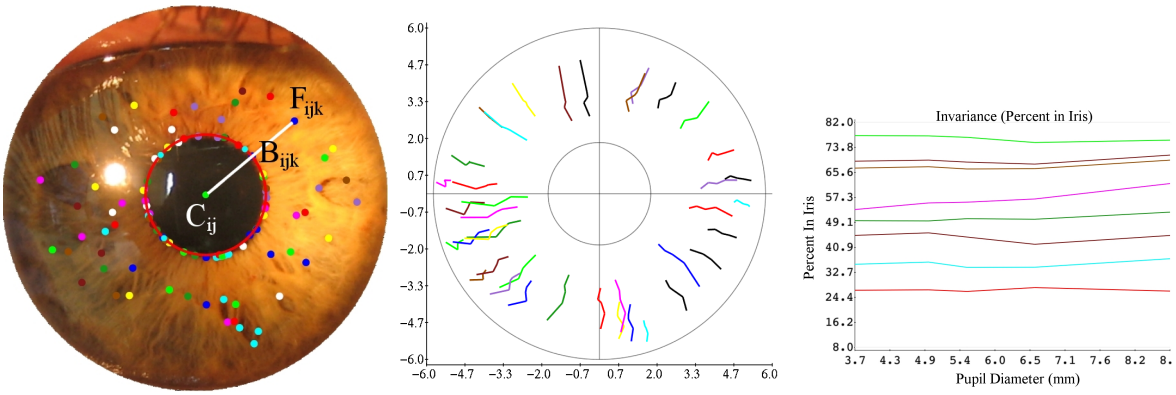

Figura B.5: Esquerda: Fotografia da íris de um voluntário durante o processo de dilatação. Os pontos coloridos indicam as saliências analisadas. Centro: Um gráfico mostrando o comportamento de cada ponto analisado durante a dilatação da pupila. Direita: Um gráfico que apresenta, em percentual, a posição de um subconjunto das saliências relativo a largura da íris. Nota-se, através destes gráficos que as saliências se movem radialmente e mantem constante a sua posição relativa a largura da íris.

A animação da deformação dos padrões radiais é feita usando uma malha em *triangle-strip* sobre um disco definido por dois círculos que delimitam a íris (Figura B.6 baixo) e com uma fotografia de uma íris com uma pupila pequena como textura. As coordenadas de textura do círculo interno são mapeadas a borda da pupila e as do círculo externo para a borda da íris. A animação modifica a posição dos pontos da borda interna, aumentando o diminuindo o raio do círculo que a define, sem alterar as coordenadas de textura.

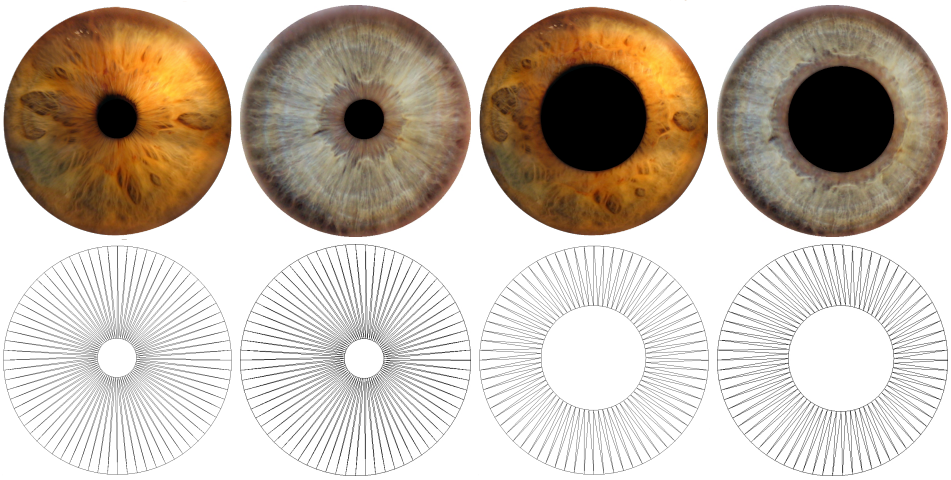

Figura B.6: Exemplos de íris renderizadas usando o modelo proposto para dilatação e contração e para deformação dos padrões. Cima: imagens geradas a partir de intensidades de luz de 10^5 blondels (esquerda) e 1 blondel (direita). Baixo: malhas de triangulos usadas para renderizar.

Figura B.7 mostra o resultado do modelo de deformação criado comparando imagens reais com imagens produzidas pelo modelo.

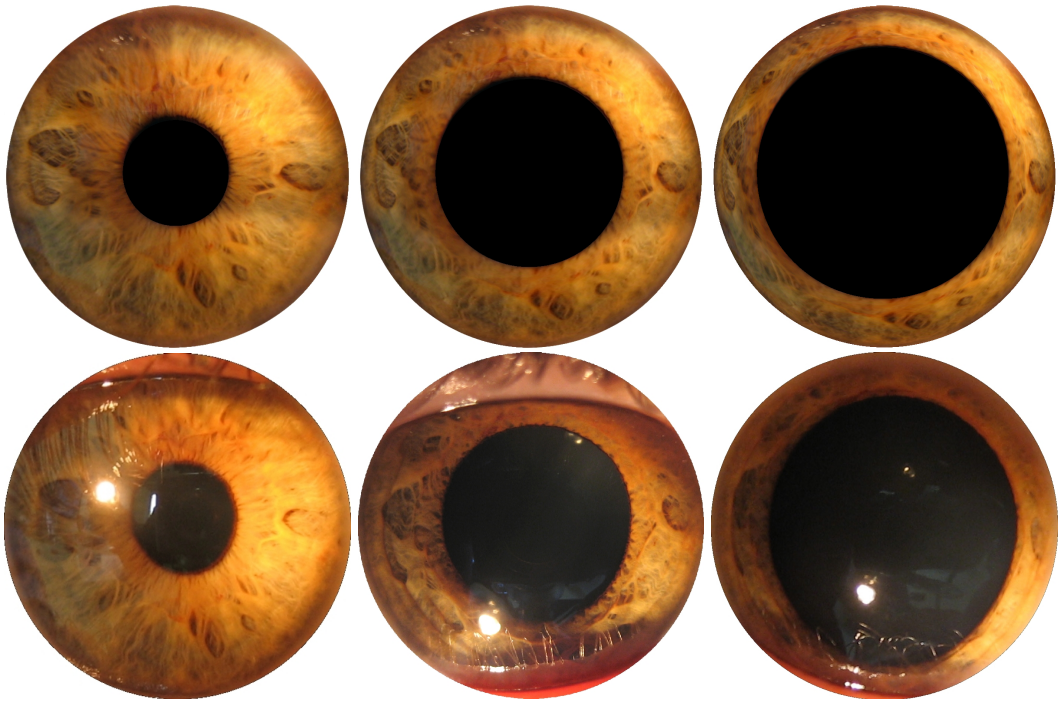

Figura B.7: Comparação dos resultados produzidos pelo modelo proposto com um conjunto de fotografias. Cima: imagens renderizadas usando o modelo de deformação de padrões para ambientes iluminados com $35,638.70$ e $2,928.78$ lumens/mm^2, respectivamente, para as duas primeiras imagens. A terceira simula uma indução por medicamento. Baixo: fotografias da íris humana com diferentes diâmetros pupilares.

B.4 Conclusões

Esta dissertação apresenta novos modelos para síntese realista do comportamento da íris e pupila humana. O modelo para reflexo pupilar em função da luz combina e estende resultados teóricos com dados experimentais coletados por vários pesquisadores. O modelo resultante é expressado em termos de uma equação diferencial com atraso que descreve as mudanças no diâmetro pupilar em função da iluminação ambiente. O modelo é original no sentido de simular as diferenças individuais e a Hippus em função da iluminação. Os modelos foram validados através de comparações dos resultados simulados com fotografias e vídeos capturados de íris humanas. A qualidade da predição ultrapassou as nossas expectativas, dado o pequeno número de parâmetros envolvido.

Até onde sabemos, o nosso modelo fisiológico é o primeiro a simular o PLR da literatura de computação gráfica. É o primeiro modelo prático na literatura para simular a dinâmica da pupila e íris em condições de iluminação não constantes e o primeiro modelo integrado em toda a literatura a considerar variabilidade individual usando equações gerais para latência, velocidade e hippus. Nosso modelo para deformação é também o primeiro modelo deste tipo na área de computação gráfica. Nossos resultados deveriam encontrar aplicabilidade imediata em diversas áreas que requerem animações faciais com alto detalhe, como em filmes de animação, onde a busca por cenas mais realistas nunca termina.

Livros Grátis

(http://www.livrosgratis.com.br)

Milhares de Livros para Download:

Baixar livros de Administração
Baixar livros de Agronomia
Baixar livros de Arquitetura
Baixar livros de Artes
Baixar livros de Astronomia
Baixar livros de Biologia Geral
Baixar livros de Ciência da Computação
Baixar livros de Ciência da Informação
Baixar livros de Ciência Política
Baixar livros de Ciências da Saúde
Baixar livros de Comunicação
Baixar livros do Conselho Nacional de Educação - CNE
Baixar livros de Defesa civil
Baixar livros de Direito
Baixar livros de Direitos humanos
Baixar livros de Economia
Baixar livros de Economia Doméstica
Baixar livros de Educação
Baixar livros de Educação - Trânsito
Baixar livros de Educação Física
Baixar livros de Engenharia Aeroespacial
Baixar livros de Farmácia
Baixar livros de Filosofia
Baixar livros de Física
Baixar livros de Geociências
Baixar livros de Geografia
Baixar livros de História
Baixar livros de Línguas